The Hα Broadband Photometric Reverberation Mapping of Four Seyfert 1 Galaxies

Qinchun Ma[1,2] , Xue-Bing Wu[1,2] , Huapeng Gu[1,2], Yuhan Wen[1,2], and Yuming Fu[1,2]

[1] Department of Astronomy, School of Physics, Peking University, Beijing 100871, People's Republic of China; maqinchun@pku.edu.cn
[2] Kavli Institute for Astronomy and Astrophysics, Peking University, Beijing 100871, People's Republic of China; wuxb@pku.edu.cn

Abstract

Broadband photometric reverberation mapping (PRM) has been investigated for active galactic nuclei (AGNs) in recent years, but mostly on accretion disk continuum RM. Due to the small fraction of broad emission lines in the broad band, PRM for emission lines is very challenging. Here, we present an ICCF-Cut method for broadband PRM to obtain the Hα broad-line lag and apply it to four Seyfert 1 galaxies: MCG+08-11-011, NGC 2617, 3C 120, and NGC 5548. All of them have high-quality broadband lightcurves with daily/subdaily cadences, which enable us to extract Hα lightcurves from the line band by subtracting the contributions from the continuum and host galaxy. Their extracted Hα lightcurves are compared with the lagged continuum-band lightcurves, as well as the lagged Hβ lightcurves obtained by spectroscopic RM (SRM) at the same epochs. The consistency of these lightcurves and the comparison with the SRM Hβ lags provide support for the Hα lags of these AGNs, in a range from 9 to 19 days, obtained by the ICCF-Cut, JAVELIN, and χ^2 methods. The simulations for evaluating the reliability of the Hα lags and the comparisons between the SRM Hβ and PRM Hα lags indicate that the consistency of the ICCF-Cut, JAVELIN, and χ^2 results can ensure the reliability of the derived Hα lags. These methods may be used to estimate the broad-line region sizes and black hole masses of a large sample of AGNs in large multi-epoch, high-cadence photometric surveys such as LSST in the future.

Unified Astronomy Thesaurus concepts: Reverberation mapping (2019); Seyfert galaxies (1447); Active galactic nuclei (16)

1. Introduction

Active galactic nuclei (AGNs) are powered by the accretion processes onto central supermassive black holes (SMBHs; Urry & Padovani 1995). Surrounding the SMBH is the geometrically thin, optically thick accretion disk, which generates the UV/optical continuum emission. The continuum light from the central accretion disk travels across the broad-line region (BLR), and produces broad emission lines through the photoionization process. AGNs often show large and aperiodic variabilities in all the wave bands, but the origins of these are still not very clear. Several models, including accretion disk instabilities (Kawaguchi et al. 1998) and the general Poisson process models (Cid Fernandes et al. 2000), have been proposed for characterizing the optical variability of AGNs.

Reverberation mapping (RM; Blandford & McKee 1982; Peterson 1993) exploits the time delay τ between the lightcurves of the optical continuum and broad emission lines to study the size and structure of the BLR. The average size of the BLR is $R_{\mathrm{BLR}} = \tau \cdot c$, where c is the speed of light. This method has been proved powerful for estimating the virial mass of the central SMBH:

$$M_{\mathrm{BH}} = f \frac{R_{\mathrm{BLR}} \cdot \sigma_v^2}{G}, \qquad (1)$$

where σ_v is the velocity dispersion of the broad emission line that can be estimated from the spectrum, G is the gravitational constant, and f is a dimensionless factor of order of unity that depends on the geometry and kinematics of the BLR (Peterson & Wandel 1999;

Onken et al. 2004; Labita et al. 2006; Woo et al. 2010; Graham et al. 2011). The factor f can be estimated for nearby AGNs whose M_{BH} values have been obtained by both RM and the correlation between M_{BH} and the stellar velocity dispersion (Collin et al. 2006; Woo et al. 2015).

RM has established an empirical relationship between the BLR size and the AGN continuum luminosity (Kaspi et al. 1996, 2000; Bentz et al. 2006, 2009), $R_{\mathrm{BLR}} \propto L^{\alpha}$. The theoretical prediction from the photoionization model gives $\alpha = 0.5$ (Netzer 1990), which has been examined extensively by many observational campaigns (Koratkar & Gaskell 1991; Kaspi et al. 1996; Wandel et al. 1999; McGill et al. 2008; Vestergaard et al. 2011; Shen et al. 2015; Grier et al. 2017). However, a large number of accurate measurements of R_{BLR} are required to reduce the scatter of the current $R - L$ relation. Because the sizes of BLRs usually range from a few to several hundred light days and the observed time lags are the product of the rest-frame time lags and the time dilation factor $1 + z$, monitoring the variability of AGNs can take months to years. Spectroscopic RM (SRM) monitors the spectra of AGNs to get the time delay between the continuum and the broad emission line. However, SRM campaigns are expensive, because they need a large amount of observational time from intermediate to large optical telescopes. In addition, extracting accurate lightcurves from spectroscopic observations is often difficult due to the uncertainties in the flux calibration process (Shapovalova et al. 2008; Stalin et al. 2011).

Photometric RM (PRM) employs broad bands to trace the AGN continuum and suitable narrow bands to trace the broad emission lines. With small optical telescopes, PRM can monitor AGNs with high efficiency. For example, Haas et al. (2011) used PRM with a 15 cm telescope, VYSOS-6, to obtain the BLR sizes of PG0003 + 199 and Ark 120, proving the

feasibility of the PRM method. Because the narrow bands contain both the emission lines and the underlying continuum, the contribution from the continuum in the narrow bands must be considered. Pozo Nuñez et al. (2012) computed a synthetic $H\beta$ lightcurve by subtracting a scaled broadband lightcurve from the narrowband lightcurve to measure the BLR size of 3C 120, which was very close to the value obtained with SRM (Grier et al. 2012). In addition to the narrowband PRM, Kim et al. (2019) used three intermediate-band filters to get the time lags between the continuum and the $H\alpha$ emission line of five AGNs, which are consistent with the SRM results. Jiang et al. (2016) combined the broad and intermediate bands and detected the $H\alpha$ time lags for 13 AGNs at redshift $0.2 < z < 0.4$.

While the narrow- and intermediate-band PRM methods can increase the signal-to-noise ratios of emission lines, they have to limit the range of AGN redshifts and require special filters. The broadband PRM method uses a suitable broad band to trace the strong emission line, allowing it to cover the emission line over a wide range of redshifts. Some previous works (Edri et al. 2012; Zu et al. 2016) have investigated several AGNs with the broadband PRM method. The most important advantage is that the broadband PRM method can use the multi-epoch data of large photometric sky surveys such as the Zwicky Transient Facility (ZTF; Masci et al. 2019) and the Legacy Survey of Space and Time (LSST) of the Vera C. Rubin Observatory (LSST Science Collaboration et al. 2017). Such surveys are much more efficient than the narrow- or intermediate-band PRM campaigns, which are only applicable to a few targets within a narrow redshift range. The multi-epoch data of photometric sky surveys have been widely used for continuum RM (Homayouni et al. 2019; Yu et al. 2020). They usually use the data of broad bands to calculate the continuum lags between two broad bands directly. An important issue for the broadband PRM of emission lines is that the emission line only contributes a small fraction of the total flux in the broad band, where the continuum is dominant. Therefore, the difference between the lightcurves of the line band and the continuum band is usually too small to calculate the emission-line time lag directly. We need some new methods to obtain the emission-line time lags for the broadband PRM, and to make comparisons with the SRM results to examine the methods and results.

We select four Seyfert 1 galaxies: MCG+8-11-011, NGC 2617, 3C 120, and NGC 5548, which have been widely studied from continuum RM to SRM in previous research. Fausnaugh et al. (2017) and Fausnaugh et al. (2018) presented the results of the simultaneous continuum RM and $H\beta$ SRM for MCG+8-11-011 and NGC 2617. NGC 2617 is also known as a changing-look AGN (Shappee et al. 2014) from other SRM (Feng et al. 2021) and continuum RM campaigns (Kammoun et al. 2021). 3C 120 has been widely studied with SRM (Peterson et al. 1998; Grier et al. 2012, 2013; Kollatschny et al. 2014; Hlabathe et al. 2020). Ramolla et al. (2018) used the narrow band to obtain the $H\alpha$ narrowband PRM lag for 3C 120, which is much larger than the SRM $H\alpha$ lag at a different time epoch, mainly due to the much higher luminosity in this period. NGC 5548 is one of the best-studied AGNs, with many RM campaigns in past decades (Peterson 1993; Peterson et al. 2002; Bentz et al. 2007; Denney et al. 2009; Bentz et al. 2010; Lu et al. 2016; Landt et al. 2019; Horne et al. 2021). The AGN Space Telescope and Optical Reverberation Mapping Project (Fausnaugh et al. 2016; Pei et al. 2017) has done multiwavelength photometric and simultaneous spectroscopic observations of NGC 5548.

This paper is arranged as follows. We describe the target selections in Section 2. The methods for calculating the time lags are presented in Section 3. The calculated $H\alpha$ lag results for the four Seyfert 1 galaxies are presented in Section 4. We use the simulations and other methods to evaluate the influences of the $H\beta$ and inter-continuum lags in Section 5. A summary is given in Section 6. We adopt the standard ΛCDM cosmology, with $\Omega_m = 0.32$, $\Omega_\Lambda = 0.68$, and $H_0 = 67 \, \mathrm{km \, s^{-1} \, Mpc^{-1}}$ (Planck Collaboration et al. 2014) in this paper.

2. Target Selections

Broadband PRM requires at least two broadband lightcurves with high photometric accuracy and high observational cadence for AGNs. One band is the continuum band, which does not contain strong broad emission lines, and the other band is the line band, with a strong emission line. To examine our methods and results, we select AGNs with both multiband photometric observations and simultaneous SRM results, so that we can compare the time lags and the shapes of the lightcurves of broadband PRM with the time lags and lightcurves of the SRM. Because the $H\alpha$ line is much stronger than the $H\beta$ line, obtaining the $H\alpha$ time lag is more feasible for broadband PRM. The best way is to use the data of the $H\alpha$ SRM campaigns to compare the broadband PRM $H\alpha$ time lags and lightcurves with the SRM results. However, the number of $H\alpha$ SRM campaigns is much smaller than the number of $H\beta$ SRM campaigns, and these $H\alpha$ SRM campaigns do not have enough photometric broadband observations or their photometric lightcurves do not have the high accuracy and high cadence that are necessary for broadband PRM. Finally, we select four Seyfert 1 galaxies with simultaneous high-quality continuum RM and $H\beta$ RM observations. We use the photometric data to obtain the time lags and lightcurves of the $H\alpha$ line and compare these results with their SRM $H\beta$ time lags and lightcurves.

Table 1 shows properties including the photometric durations, the epochs of the line and continuum bands, the cadences and the rms variability fractions (F_{var}) for four Seyfert 1 galaxies. The data of MCG+8–11–011 and NGC 2617 are obtained from Fausnaugh et al. (2018) and Fausnaugh et al. (2017). The data of 3C 120 are obtained from Hlabathe et al. (2020). These three targets were observed with the Las Cumbres Observatory (LCO; Brown et al. 2013) global robotic telescope network. The data of NGC 5548 are obtained from Fausnaugh et al. (2016) and Pei et al. (2017). Their $H\alpha$ ratios are calculated from the single-epoch spectra shown in Figure 1. The transfer functions of the continuum bands and the line bands used in the broadband PRM for the four galaxies are also shown in Figure 1. Because the spectrum of the simultaneous $H\beta$ SRM cannot cover the whole wavelength range of the line band, we use the single-epoch spectra from other observations and campaigns as substitutes. The spectrum of NGC 2617 is obtained from Feng et al. (2021). The spectrum of 3C 120 is obtained from Ramolla et al. (2018). The spectrum of NGC 5548 is obtained from the Sloan Digital Sky Survey (SDSS; York et al. 2000). We obtain the single-epoch spectrum of MCG+8-11-011 using the Beijing Faint Object Spectrograph and Camera of the Xinglong 2.16 m telescope in China. We use the Grism 4 with a dispersion of 198 Å mm^{-1} and the slit width of $1''.8$. The spectra are reduced by the standard IRAF routine (Tody 1986, 1993).
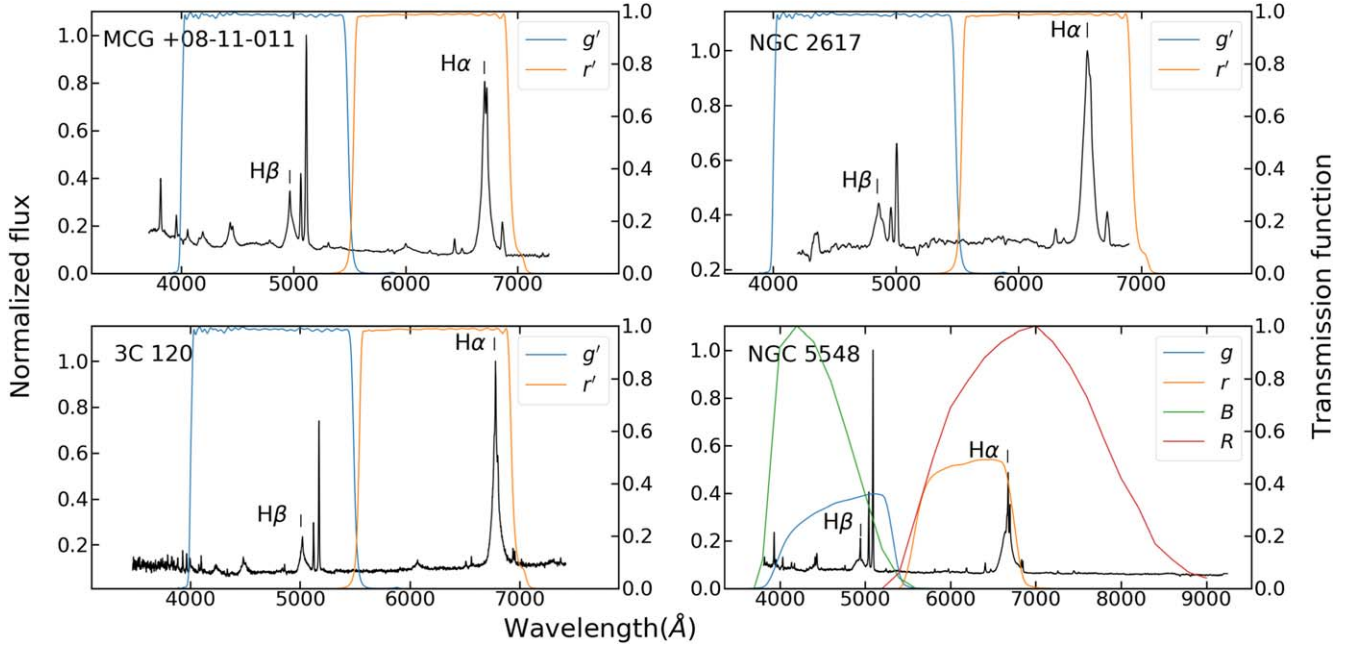
Figure 1. The spectra of four Seyfert 1 galaxies and the transmission functions of the broad bands used for broadband PRM. The g, g', and B bands are used for the continuum bands, and the r, r', and R bands are used to extract the Hα line.

Table 1
The Properties for Four Seyfert 1 Galaxies

Name	Redshift	Hα Ratio(%)	Band	Duration (days)	Epoch	Cadence (days)	F_{var} (%)
MCG+8-11-011	0.0205	26	r'	93	42	1.07	4.8
			g'	156	85	1.00	7.0
NGC 2617	0.0142	16	r'	102	127	0.62	3.7
			g'	145	166	0.69	3.8
3C 120	0.0330	23	r'	249	370	1.08	6.3
			g'	246	392	1.06	9.1
NGC 5548	0.0172	25	r	212	203	0.93	3.5
			g	212	204	0.98	6.2
		19	R	226	161	0.96	3.7
			B	225	180	1.00	8.6

We use the LCO g' band as the continuum band and the r' band as the line band for MCG+8-11-011, NGC 2617, and 3C 120. For NGC 5548, besides the SDSS g and r bands, we also use the Johnson/Cousins B and R bands to do the broadband PRM as a comparison. Table 1 and Figure 1 show that all of them have very high photometric cadences and strong Hα emission lines for the broadband PRM (we will not distinguish g' and r' from g and r afterward).

3. Time Lag Calculations

3.1. The ICCF-Cut Method

The interpolated cross-correlation function (ICCF; Gaskell & Sparke 1986) calculates the time lag between two different lightcurves directly and has been extensively used in SRM. To get the emission-line time lag of the broadband PRM, we need to get rid of the continuum contribution in the line band. First, we simply assume that the continuum flux in the line band equals a fixed fraction α of the flux in the continuum band for each AGN. Under this assumption, we use the line-band flux to subtract the continuum-band flux with the ratio α, and get the

lightcurve of the Hα line (hereafter, ICCF-Cut):

$$L_{\mathrm{H\alpha}}(t) = L_{\mathrm{line}}(t) - \alpha L_{\mathrm{cont}}(t). \qquad (2)$$

Here, $L_{\mathrm{line}}(t)$, $L_{\mathrm{cont}}(t)$, and $L_{\mathrm{H\alpha}}(t)$ are the lightcurves of the line band, continuum band, and Hα emission line, respectively. We ignore the influence of Hβ variability in the continuum band because the Hβ emission line usually contributes less than 5% in the continuum band and is much weaker than the Hα emission line (which has a $10\% \sim 30\%$ contribution to the line band). According to the thin-disk model, there is a small inter-continuum time lag between the continuum in the g and r bands. Because the inter-continuum lag is usually very small for lower-redshift Seyfert 1 galaxies (Fausnaugh et al. 2016, 2018), we ignore the influence of the inter-continuum lag between the line band and continuum band at first. Further simulation and discussion of the influence of the Hβ emission line and the inter-continuum lag will be presented in Section 5. The value of α is associated with the spectral slope of the AGN continuum and usually does not change much within several months. We use the spectral data of the Lick AGN Monitoring Project (Bentz et al. 2010) to examine the variability of α and find that α changes little during the campaign
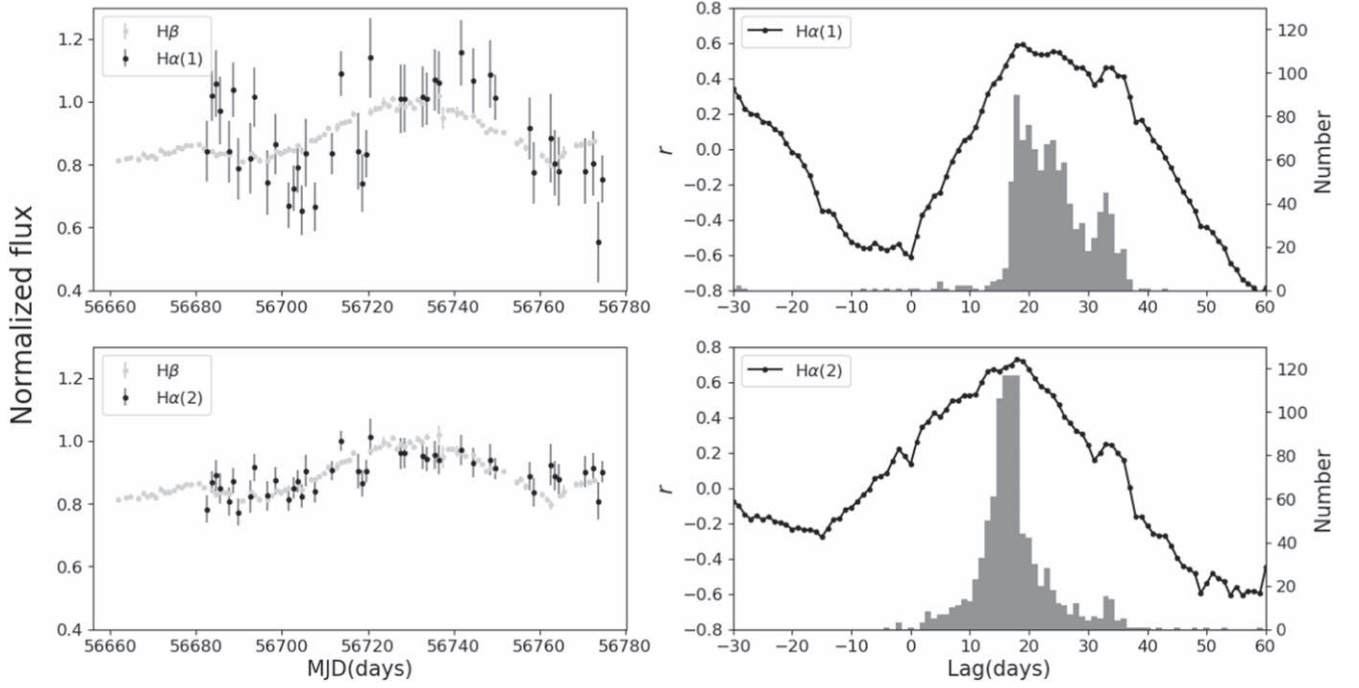
Figure 2. The SRM Hβ and extracted Hα lightcurves and the ICCF-Cut lag distributions of MCG+8-11-011 with the $15.7^{+0.5}_{-0.5}$ days SRM Hβ lag. The left panel shows the Hβ and extracted Hα emission-line lightcurves with different methods. The gray points represent the Hβ lightcurves. The labels Hα(1) and Hα(2) represent the cases using Equations (3) and (4), respectively. All lightcurves have been normalized and the Y-axis has been set to the same scaling for comparison. The right panel shows the ICCF-Cut lag results obtained from Hα(1) and Hα(2). The black lines represent the relations between the cross-correlation coefficient r and the time lag and the gray parts represent the 1000 FR/RSS simulations that represent the lag distributions. The time lags between the g band and the Hα line for Hα(1) and Hα(2) are $23.8^{+8.2}_{-4.8}$ and $17.3^{+6.2}_{-4.3}$ days, respectively.
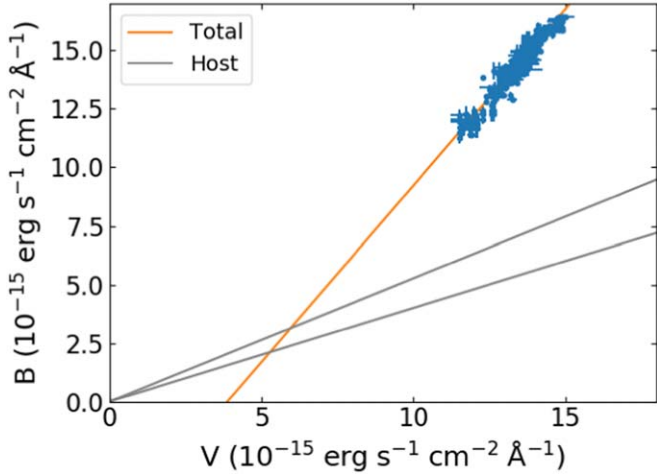

Figure 3. The B- vs. V-band fluxes of NGC 5548. A linear least-squares fit to the data points yields the AGN slope plotted by the orange line. The range of host slopes plotted by the two gray lines is taken from Sakata et al. (2010).
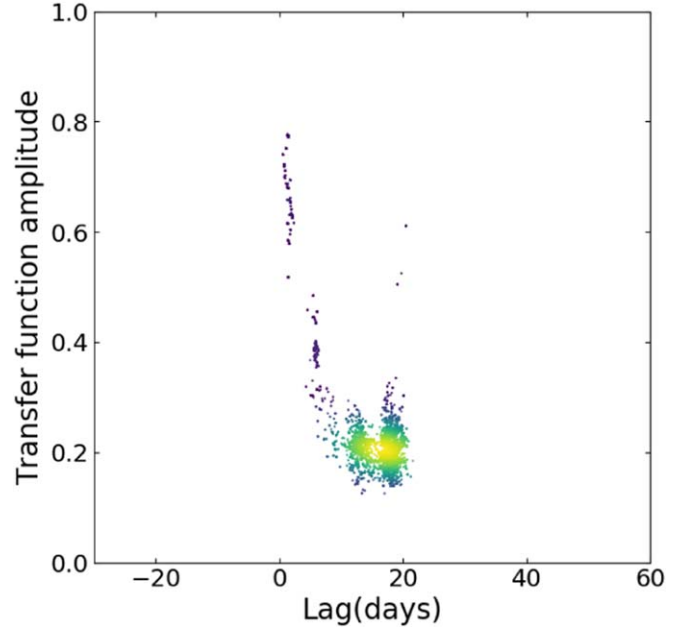

Figure 4. The time lags and the transfer function amplitude distribution of the JAVELIN Pmap model results for MCG+8-11-011, whose SRM Hβ lag is $15.72^{+0.50}_{-0.52}$ days. The color represents the number density of the points. The JAVELIN Hα lag is $17.3^{+1.5}_{-5.2}$ days.

(e.g., $\alpha = 1.02 \pm 0.07$ for NGC 4748, and $\alpha = 1.16 \pm 0.09$ for Arp 151).

The α value can be obtained from the transmission functions of the line and continuum-band filters and the single-epoch spectrum of an AGN. Because the spectra of simultaneous Hβ SRM for these targets cannot cover the entire wavelength range of the line band, we use the single-epoch spectra in Figure 1 to calculate α:

$$\alpha = (F_{\text{line}} - F_{\text{H}\alpha})/F_{\text{cont}}. \qquad (3)$$

Here, F_{cont}, F_{line}, and $F_{\text{H}\alpha}$ are the fluxes obtained from the integral of the single-epoch spectrum. However, there are two issues. One

is that the flux calibration of the spectrum is usually not as accurate as the photometric flux calibration. Another one is that these spectroscopic and photometric observations have been conducted at different epochs (several years apart from each other), so the spectral index of the AGN continuum and the value
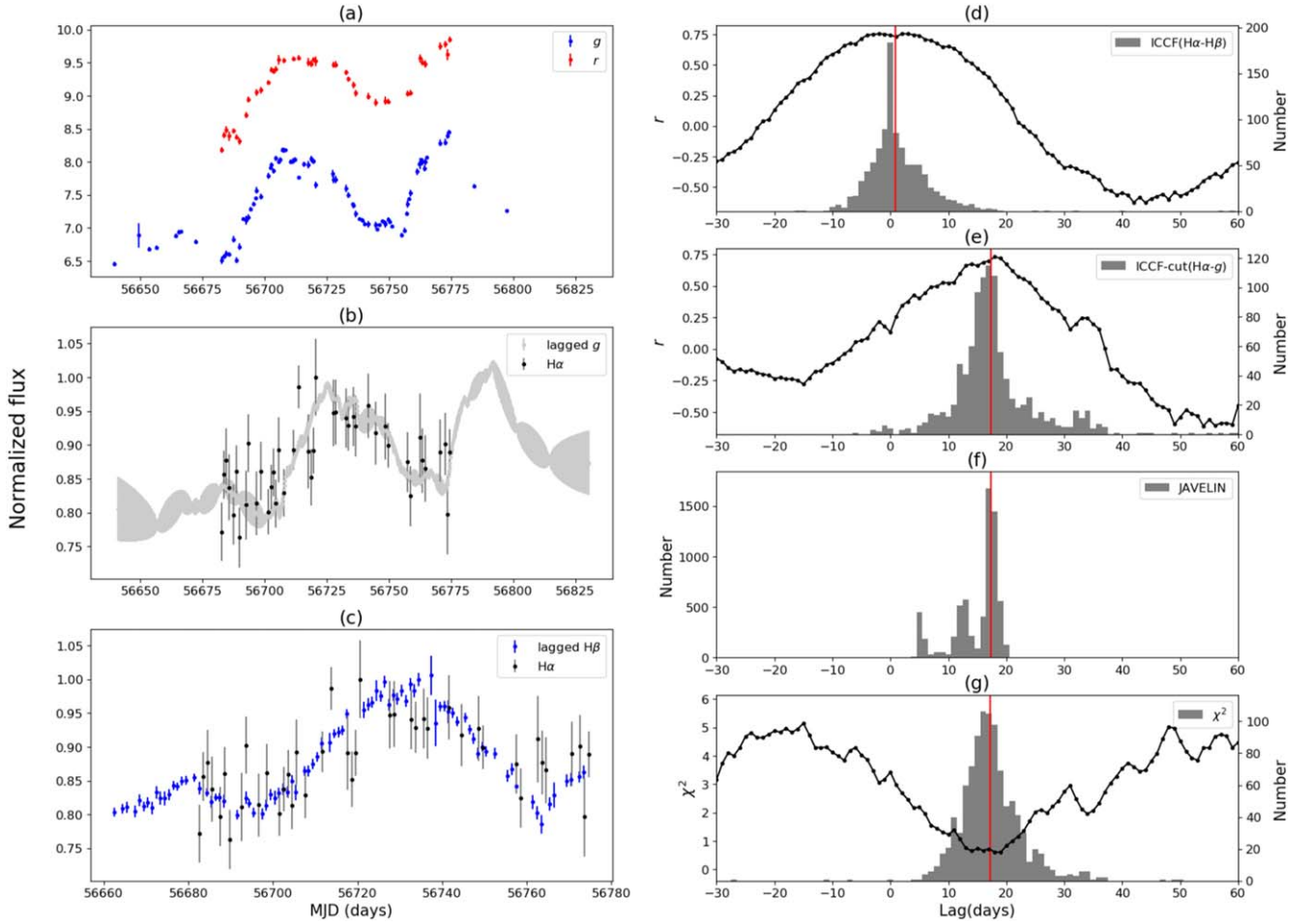
Figure 5. The lightcurves and lag distributions for MCG+8-11-011. Panel (a) shows the lightcurves of the continuum band (*g*) and line band (*r*). Panels (b) and (c) show the extracted Hα lightcurves compared with the lagged continuum-band and SRM Hβ broad-line lightcurves. Panel (d) shows the lag distribution between the SRM Hβ line and extracted Hα line. Panels (e), (f), and (g) show the lag distributions of the continuum band and extracted Hα line with the ICCF-Cut, JAVELIN, and χ^2 methods, respectively. The red line represents the median value of the lag distribution. For the two ICCF results, the black lines represent the relations between the cross-correlation coefficient *r* and the time lag. For the χ^2 results, the black line represents the relation between the χ^2 value and the time lag. The gray parts of these three panels (d), (e), and (g) represent the 1000 FR/RSS simulations. The gray part of the JAVELIN results (panel (f)) represents the distributions of 10,000 MCMC simulations.

of α may change significantly. Here, we adopt another method to calculate the value of α for the broadband PRM. We assume the average contribution of the Hα line in the line band does not change much between the spectroscopic epoch and the mean epoch of the photometric lightcurves. To make sure the extracted Hα lightcurve contains all the contributions of the Hα emission line, we use the minimum function

$$\alpha = \left(1 - \frac{F_{\mathrm{H}\alpha}}{F_{\mathrm{line}}}\right)\min\left(\frac{L_{\mathrm{line},t}}{L_{\mathrm{cont},t}}\right) \qquad (4)$$

to calculate the value of α. Here, $F_{\mathrm{H}\alpha}$ and F_{line} are measured from the single-epoch spectrum, and $L_{\mathrm{line},t}$ and $L_{\mathrm{cont},t}$ are the fluxes at each point obtained from linear interpolated photometric light-curves. For the single-epoch spectrum and two broadband lightcurves, we calculate the α value using Equation (4) and use it for the observational period. In this case, adopting the minimum as the α value means that the contribution of Hα in the line band for each point of the photometric lightcurve will be kept and be larger than the contribution obtained directly from the single-epoch spectrum. However, we can still exclude a large

fraction of continuum in the line band, while keeping the Hα contribution as complete as possible. We will discuss the influence of the varying value of α in Section 6.

Here, we investigate the difference in the results of applying Equations (3) and (4) to obtain the value of α. Figure 2 shows an example of a comparison between the results derived from two different α values given by the two approaches above for MCG+8-11-011. By comparing the lightcurves of the extracted Hα and the SRM Hβ lines, we find that the extracted Hα lightcurve using Equation (4) is more consistent with the SRM Hβ lightcurve. The value of the cross-correlation coefficient *r* from using Equation (4) is higher and the lag distribution is smoother than from using Equation (3). This indicates that the result obtained from Equation (4) is more reliable. When using Equation (3), the extracted Hα lightcurves do not contain enough contribution of the real Hα line variability to obtain the time lag. This comparison indicates that using Equation (4) to calculate the value of α is more suitable for obtaining the Hα lightcurves and time lags for the broadband PRM.

We also consider the influence of the host galaxy. The luminosity of the host galaxy changes little for the RM campaign
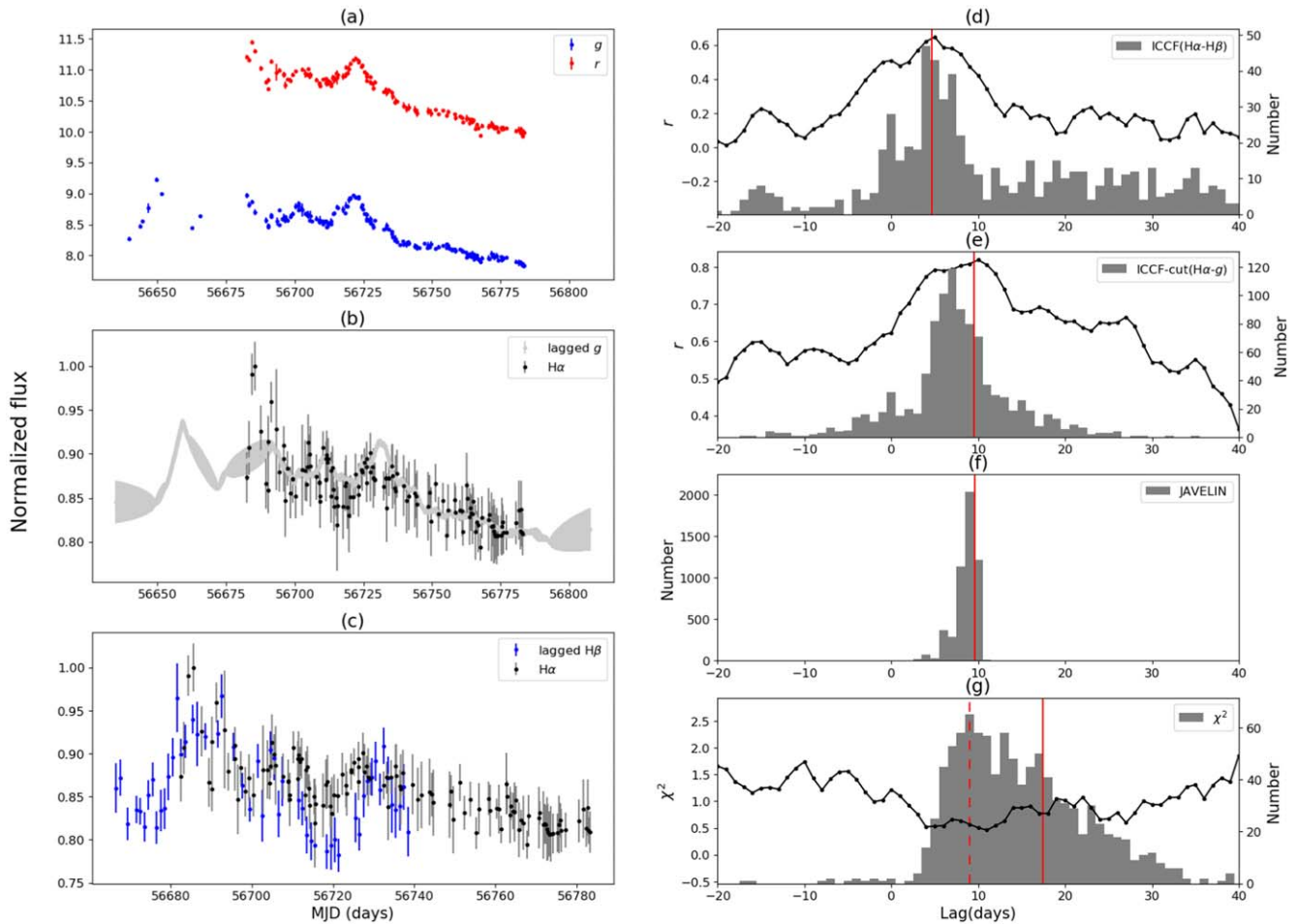
Figure 6. Same as Figure 6, but for NGC 2617. The red dashed line in panel (g) represents the peak value of the χ^2 lag distribution. The red solid lines represent the median lags of the distributions.

durations, so it can be regarded as constant for most SRM campaigns. The shapes of the lightcurves do not change with the host galaxy contribution for SRM and narrowband PRM (Pozo Nuñez et al. 2013; Ramolla et al. 2018). But for broadband PRM, the contribution of the host galaxy can change the value of α and then affect the shape of the extracted Hα lightcurves. Its contribution must be considered. We use the flux variation gradient (Choloniewski 1981; Winkler et al. 1992; Pozo Nuñez et al. 2012) to determine the contribution of the host galaxy. As shown in Figure 3, we obtain the host galaxy contributions in the B and V bands for NGC 5548. They are 2.6 ± 0.5 and 5.6 ± 0.3 in units of $10^{-15} \, \mathrm{erg \, s^{-1} \, cm^{-2} \, \mathring{A}^{-1}}$ for the B and V bands, respectively, which are consistent with the results in Fausnaugh et al. (2016; 2.88 ± 0.05 and 5.25 ± 0.10).

The host galaxy contributions to the g, r, and R bands can be estimated from the B- and V-band values by using the host galaxy template (Polletta et al. 2007). A similar method is also applied to the other three AGNs to estimate the host contributions to the continuum and line bands.

3.2. The JAVELIN Method

To check the reliability of the time lag calculated by the ICCF-Cut method, we also use another method to calculate the time lags of AGNs as a comparison. The Just Another Vehicle for Estimating Lags In Nuclei (JAVELIN: Zu et al. 2011,

2013, 2016) program assumes that the lightcurves of AGNs can be modeled by a damped random walk (DRW) process and uses thousands of Markov Chain Monte Carlo (MCMC) DRW processes to get the distributions of the parameters, including the time lag. Because the two-band photometry model (Pmap Model) of JAVELIN may be competitive with the SRM for strong (large equivalent width) lines such as Hα and Hβ (Zu et al. 2016), we can use JAVELIN to calculate the time lag of AGNs with strong Hα emission lines. From the time lag distribution of JAVELIN, we use the highest posterior density to identify the time lag. The 1σ limits of the time lag that encompass 68% of the time lag distribution are adopted to obtain the upper and lower limits of the most probable time lag. To make sure the results of JAVELIN are reliable, in addition to the lag distribution, the transfer function amplitude between the continuum and the Hα emission line in the DRW model is also examined for the broadband PRM. The transfer function amplitude can represent the statistical mean of the Hα line contribution in the line band. A lag with a much higher transfer function amplitude than the real Hα line ratio in the spectrum is not physically possible. Combining the distribution of lags and the transfer function amplitude, we can evaluate the reliability of the lag results.

Figure 4 shows the time lags and the transfer function amplitude distribution of the JAVELIN Pmap model results for MCG+8-11-011. The transfer function amplitude (on average
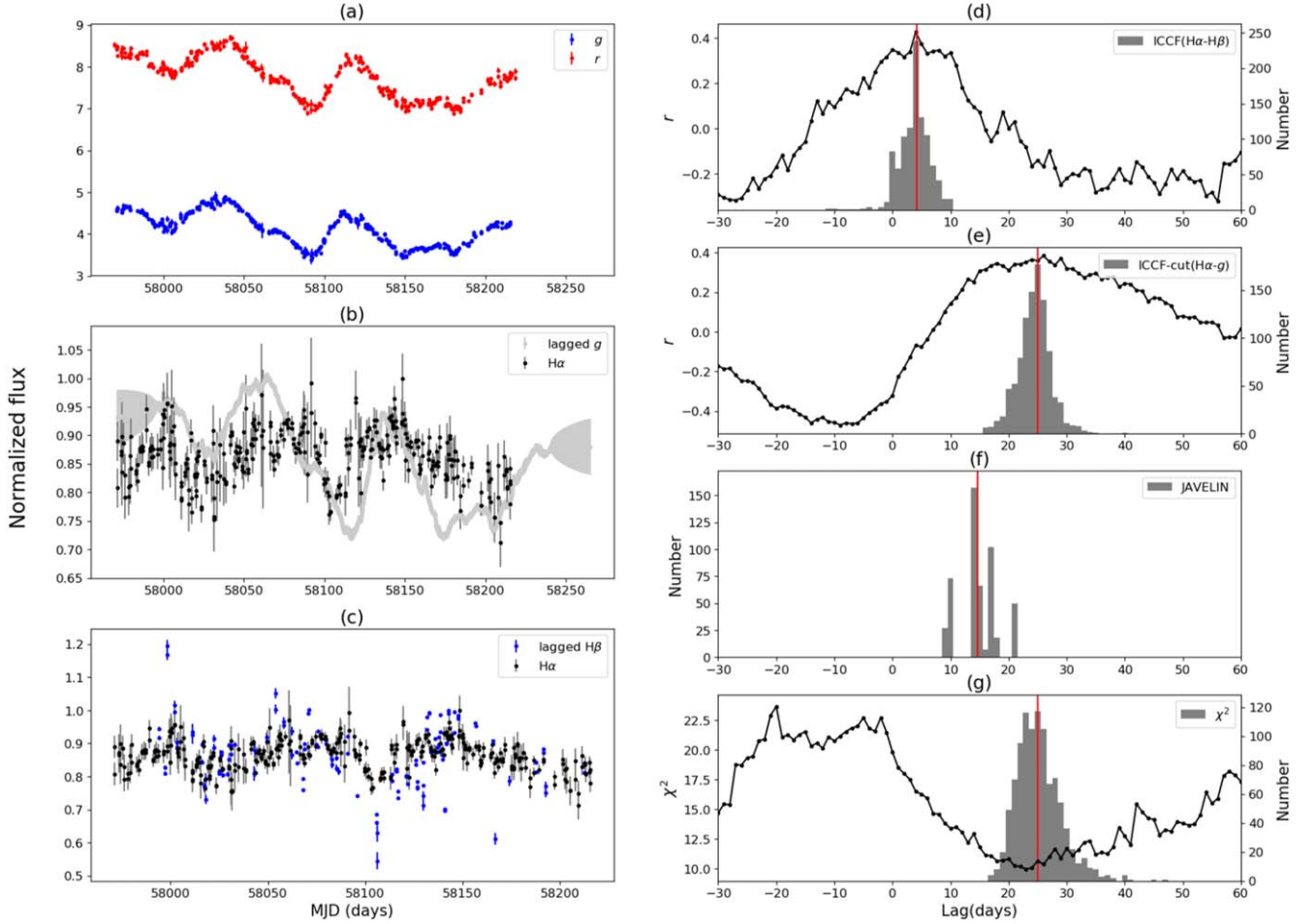
Figure 7. Same as Figure 6, but for 3C 120 without lightcurve segmentation.

~23%) can represent the Hα line ratio in the line band. It is consistent with the real Hα line ratio (26%) calculated from the single-epoch spectrum. MCG+8-11-011 has an SRM Hβ lag of $15.72^{+0.50}_{-0.52}$ days, while the JAVELIN Hα time lag of $17.3^{+1.5}_{-5.2}$ days is consistent with the ICCF-Cut Hα result of $17.3^{+6.2}_{-4.3}$ days. The Hα time lag is slightly larger than the SRM Hβ time lag, which is consistent with the structure of BLR and the results of previous works (Kaspi et al. 2000; Bentz et al. 2010; Grier et al. 2012). We notice that the lags of a few points are close to zero with much higher transfer function amplitude (see Figure 4), which may be because the JAVELIN MCMC processes need a higher line ratio as the time lag decreases to reproduce the given line-band flux. To reduce such influence, we exclude the points with a transfer function amplitude larger than 0.4 and the lag results are very close to zero.

3.3. The χ^2 Method

From the comparison of the lightcurves in panels (b) and (c) of Figure 5, it can be noticed that the errors of the extracted Hα are much larger than the errors of the photometric broad bands and SRM Hβ lightcurves. To evaluate the influence of errors and the feasibility of the broadband PRM with large errors, we also apply the χ^2 method (Czerny et al. 2013; Bao et al. 2022), which works better than the ICCF for AGNs with red-noise variability in obtaining the Hα time lag from the broadband and extracted Hα lightcurves.

The χ^2 method uses the uncertainties to weight the data points in lightcurves. The χ^2 is calculated by

$$\chi^2(\Delta t) = \frac{1}{N}\sum_{i=1}^{n} \frac{(x_i - A_{\chi^2} y_{i,\Delta t})^2}{\delta x_i^2 + A_{\chi^2}^2 \delta y_{i,\Delta t}^2}, \quad (5)$$

where x_i and $y_{i,\Delta t}$ are the continuum-band flux and the extracted Hα flux with shifted lag Δt, while δx_i and $\delta y_{i,\Delta t}$ are their uncertainties. We interpolate and shift the extracted Hα flux with the time Δt. For each line flux with the shifted lag Δt, we can obtain the value of $\chi^2(\Delta t)$. This leads to a relation between the $\chi^2(\Delta t)$ value and time lag Δt. This process is similar to the ICCF. A_{χ^2} is a normalized factor formulated as

$$A_{\chi^2} = \frac{S_{xy} + (S_{xy}^2 + 4S_{x3y}S_{xy3})^{1/2}}{2S_{xy3}}, \quad (6)$$

where the coefficients are given by

$$S_{xy} = \sum_{i=1}^{N}(x_i^2 \delta y_{i,\Delta t}^2 - y_{i,\Delta t}^2 \delta x_i^2),$$

$$S_{xy3} = \sum_{i=1}^{N} x_i y_{i,\Delta t} \delta y_{i,\Delta t}^2,$$

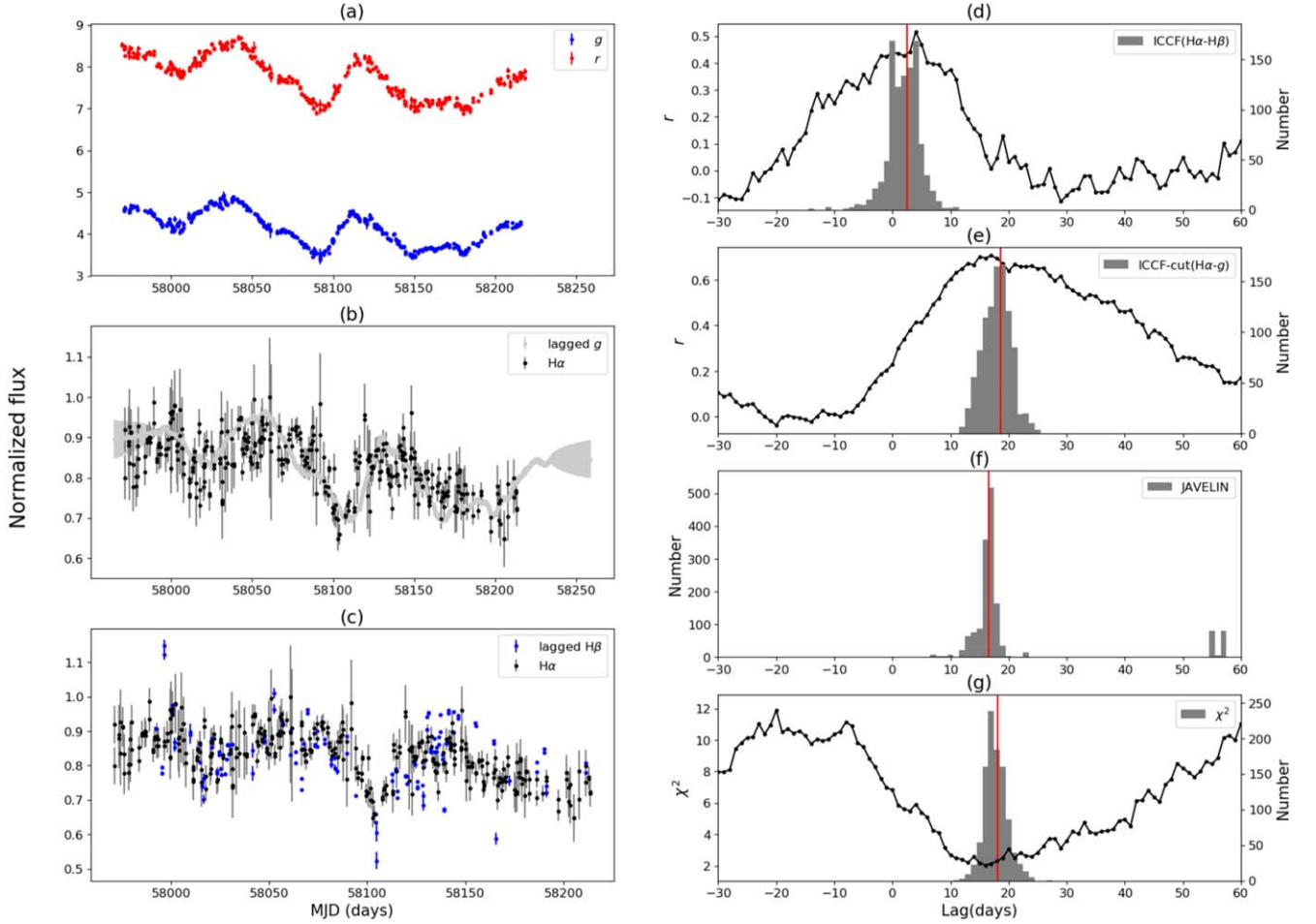$$S_{x3y} = \sum_{i=1}^{N} x_i y_{i,\Delta t} \delta x_i^2. \quad (7)$$

Figure 8. Same as Figure 6, but for 3C 120 with lightcurve segmentation into two parts at MJD 58092.

We take the minimum points in the χ^2 functions as the Hα time lag measurements.

In order to estimate the uncertainties of the time lags of ICCF-Cut and the χ^2 method, we use flux randomization (FR) and random subset selection (RSS) with Monte Carlo (MC) simulations (Peterson et al. 1998). The FR alters the flux with the errors. Each data point is modified by adding a random noise according to a Gaussian distribution around the measured value, with the standard deviation of the measurement uncertainty. The RSS is used to estimate the errors of the unevenly sampled data by randomly excluding data points from the simulated lightcurves. Each realization is based on a randomly chosen subset of the original lightcurve. The FR procedure examines the sensitivity of the flux accuracy, and the RSS checks the effect of the incomplete sampling. For each target, we perform 1000 MC simulations to get the lag uncertainty of ICCF-Cut and the χ^2 method (see panel (g) in Figure 5). The χ^2 centroid Hα time lag of $17.2^{+4.8}_{-3.9}$ days for MCG+8-11-011 is consistent with the previous ICCF-Cut and JAVELIN results, which indicates that although the uncertainties of the extracted Hα line flux are large compared with the variabilities of the lightcurves, the broadband PRM can still obtain the Hα time lag for these targets. The consistency of the Hα lag distributions from the ICCF-Cut, JAVELIN, and χ^2 methods can ensure the reliability of the Hα broadband PRM.

4. Results for Four Seyfert 1 Galaxies

We apply these methods to four Seyfert 1 galaxies. MCG+8-11-011 shows the best results, as shown in Figure 5. Besides the Hα lag calculated in the previous part, we also use the ICCF to calculate the time lag between the SRM Hβ and extracted Hα lightcurve (panel (d) of Figure 5). The high value of the coefficient r and a small lag between the SRM Hβ and subtracted Hα lightcurves confirm the reliability of the subtracted Hα lightcurves. Because the Hα ratio obtained from the single-epoch spectrum is the highest among the four galaxies and the lightcurves have obvious variabilities, the results for MCG+8-11-011 are better than for the other targets. The extracted Hα lightcurve is well consistent with the lagged continuum and the lagged SRM Hβ lightcurves. All the methods, including the ICCF-Cut, JAVELIN, and χ^2 methods, show similar lag distributions for the continuum and extracted Hα lightcurves. The Hα lag is around 17 days.

For NGC 2617, shown in Figure 6, the extracted Hα lightcurve is consistent with the lagged continuum and the lagged SRM Hβ line lightcurves. The Hα lag distributions of ICCF-Cut and JAVELIN are very close. Because the variabilities are smaller than MCG+8-11-011 compared with uncertainties, the χ^2 result is worse than those of ICCF-Cut and JAVELIN. Although the median lag of the χ^2 method is much larger than the results of ICCF-Cut and JAVELIN, the peak value $10.0^{+15.4}_{-0.2}$ days of the χ^2 method is very close to the results of ICCF-Cut and JAVELIN. Because NGC 2617 was
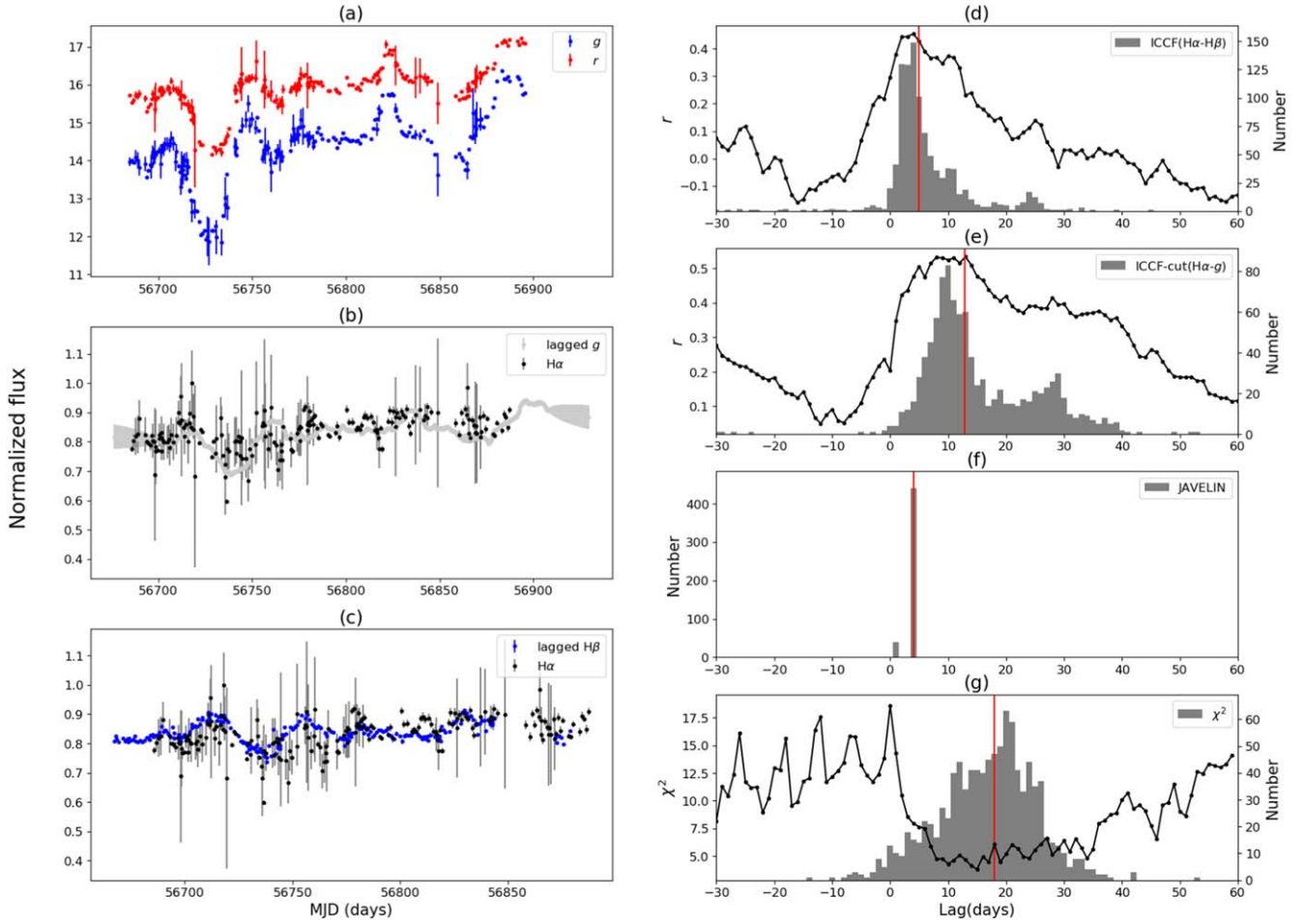
Figure 9. Same as Figure 6, but for NGC 5548 with the *g*- and *r*-band lightcurves with lightcurve segmentation into two parts at MJD 56772.

discovered by Shappee et al. (2014) to be a changing-look AGN, we abandon the SRM Hβ line lightcurve with MJD >56735 (Fausnaugh et al. 2017) for the comparisons. The latter parts of the lightcurves with lower fluxes may also be one of the reasons for the bad χ^2 result.

We apply the same methods to 3C 120, as shown in Figure 7, but the extracted Hα line lightcurve is not well consistent with the continuum band (panel (b) of Figure 7). The left part of the extracted Hα line lightcurve is obviously lower than the continuum-band lightcurve and the right part is higher. The correlation coefficient value of ICCF-Cut is also very low. We noticed that even for the simultaneous Hβ SRM, the correlation coefficient value of the ICCF between the continuum and Hβ line is also not high, only about 0.4 (Hlabathe et al. 2020). Another issue is that the observational duration of 3C 120 is about 250 days, twice the durations of MCG+8-11-011 and NGC 2617. The spectral index of the AGN continuum usually changes little within several months, as in the cases of MCG+8-11-011 and NGC 2617, but for 3C 120, the spectral index of the continuum and the value of α may change during the longer observation durations. To understand the deviation between the extracted Hα line and the continuum, we adjust Equation (4) to calculate the value of α. We divide the lightcurves into two parts, so that each part of the lightcurve has a similar duration time as MCG+8-11-011 and NGC 2617, and for each part the value of α is adjusted according to its average line-band and continuum-band fluxes.

For each part of the lightcurves, α_i is calculated by

$$\alpha_i = \alpha \frac{\overline{L_{\mathrm{cont}}}}{\overline{L_{\mathrm{line}}}} \frac{\overline{L_{\mathrm{line},i}}}{\overline{L_{\mathrm{cont},i}}}, \tag{8}$$

where $\overline{L_{\mathrm{cont}}}$ and $\overline{L_{\mathrm{line}}}$ are the average fluxes in the the continuum and line bands for the whole-period lightcurves, while $\overline{L_{\mathrm{cont},i}}$ and $\overline{L_{\mathrm{line},i}}$ are the average fluxes for each part of the lightcurves.

Figure 8 shows that for 3C 120, the subtracted Hα lightcurve with a varying α value in the two parts (separated at MJD 58092) is more consistent with the lagged continuum-band lightcurve. Similar to ICCF-Cut, we also divide the initial lightcurves into two parts to calculate the JAVELIN lags, respectively, then combine the results of the two parts into the final one. All three methods show similar lag distributions in Figure 8. Although the ICCF-Cut Hα lag of $18.6^{+2.2}_{-2.7}$ days is slightly shorter than the SRM Hβ lag of $21.2^{+1.6}_{-1.0}$ days, the time lag between the SRM Hβ line and the extracted Hα line calculated by the ICCF still shows that the extracted Hα lightcurve is possibly lagged behind the SRM Hβ lightcurve with $2.5^{+2.3}_{-3.0}$ days (panel (d) of Figure 8). This contradiction may be due to the lower accuracy of the SRM Hβ lightcurve compared with other targets. This contradiction may also be ignored because the lag uncertainties are larger than the difference between the Hα and Hβ lags. The extracted Hα lag is consistent with the SRM Hβ lag in general, which has also been found by the previous SRM research for 3C 120, showing
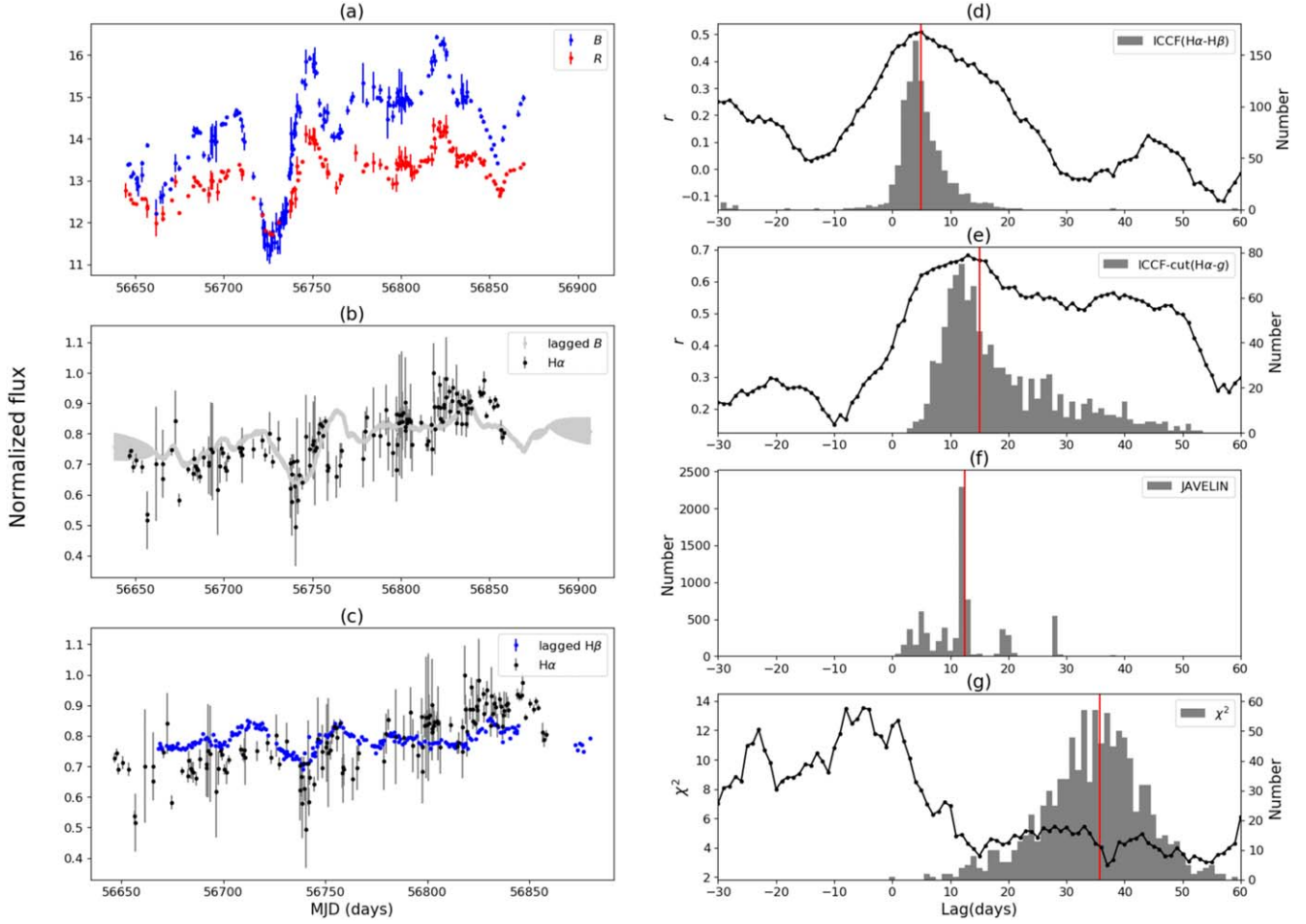
Figure 10. Same as Figure 6, but for NGC 5548 with the *B*- and *R*-band lightcurves with lightcurve segmentation into two parts at MJD 56766.

Table 2
The Hα Lag Results (in Days) of Four Seyfert 1 Galaxies

Name	ICCF-Cut	JAVELIN	χ^2	Combined	SRM Hβ	Hβ vs. Hα
MCG+8-11-011	$17.3^{+6.2}_{-4.3}$	$17.3^{+1.5}_{-5.2}$	$17.2^{+4.8}_{-3.9}$	$17.4^{+4.8}_{-3.9}$	$15.72^{+0.50}_{-0.52}$	$0.8^{+5.4}_{-4.1}$
NGC 2617	$9.5^{+9.1}_{-7.0}$	$9.6^{+0.7}_{-0.6}$	$17.5^{+7.9}_{-7.7}$	$9.0^{+7.4}_{-12.3}$	$4.32^{+1.10}_{-1.35}$	$4.7^{+3.3}_{-6.3}$
3C 120	$18.6^{+2.2}_{-2.7}$	$16.6^{+2.6}_{-3.9}$	$18.1^{+2.0}_{-1.5}$	$17.8^{+2.5}_{-1.6}$	$21.2^{+1.6}_{-1.0}$	$2.5^{+2.3}_{-3.0}$
NGC 5548 (*gr*)	$12.8^{+14.7}_{-4.8}$	$4.5^{+0.1}_{-0.2}$	$18.0^{+7.0}_{-9.3}$	$14.3^{+16.9}_{-5.8}$	$4.17^{+0.36}_{-0.36}$	$5.0^{+6.5}_{-2.5}$
NGC 5548 (*BR*)	$15.0^{+14.2}_{-5.1}$	$12.5^{+7.2}_{-6.7}$	$35.7^{+7.8}_{-8.8}$		$\cdots$	$5.0^{+4.0}_{-2.5}$

Note. The Hβ versus Hα lags are obtained from the SRM Hβ and the extracted Hα lightcurves with the ICCF. For NGC 5548, the combined lag is obtained from the lag distributions of both the *g*, *r* and *B*, *R* bands.

that its Hα lag ($28.5^{-8.5}_{+9.0}$ days) and Hβ lag ($27.9^{-5.9}_{+7.1}$ days) are very close (Kollatschny et al. 2014). The consistency of the Hα lightcurve with the lagged continuum and SRM Hβ lightcurves as well as the similar lag distributions for the three methods indicate that this α value adjustment method is effective for broadband PRM with a longer duration time.

For NGC 5548, with an observational duration of more than 200 days, we also divide the lightcurves into two parts (separated at MJD 56772 in Figure 9). The extracted Hα lightcurve is consistent with the lagged continuum band and the lagged SRM Hβ line lightcurves in general. Because the flux uncertainties of the continuum and line bands are larger than other targets, the lag distributions of the three methods are not very consistent with each other. The lag value of JAVELIN is much smaller than the others. We will use simulations to

explain such a difference in Section 5. To determine the Hα lag and examine the reliability of the broadband PRM, besides the *g* and *r* bands, we also used the *B* band as the continuum band and the *R* band as the line band (separated at MJD 56766 in Figure 10). The results of the *B* and *R* bands are similar to the results of the *g* and *r* bands, especially for the lag distributions of ICCF-Cut. Although the result of the χ^2 method is worse, the lag distributions of ICCF-Cut and JAVELIN are still similar.

Considering the simultaneous SRM Hβ lag of $4.17^{+0.36}_{-0.36}$ days (Pei et al. 2017) as the broadband PRM and the SRM Hα lag of $11.02^{+1.27}_{-1.15}$ days in the other period (Bentz et al. 2010) for NGC 5548, the lag distributions in Figure 9 and Figure 10 are probably reasonable. In particular, the lag distributions of
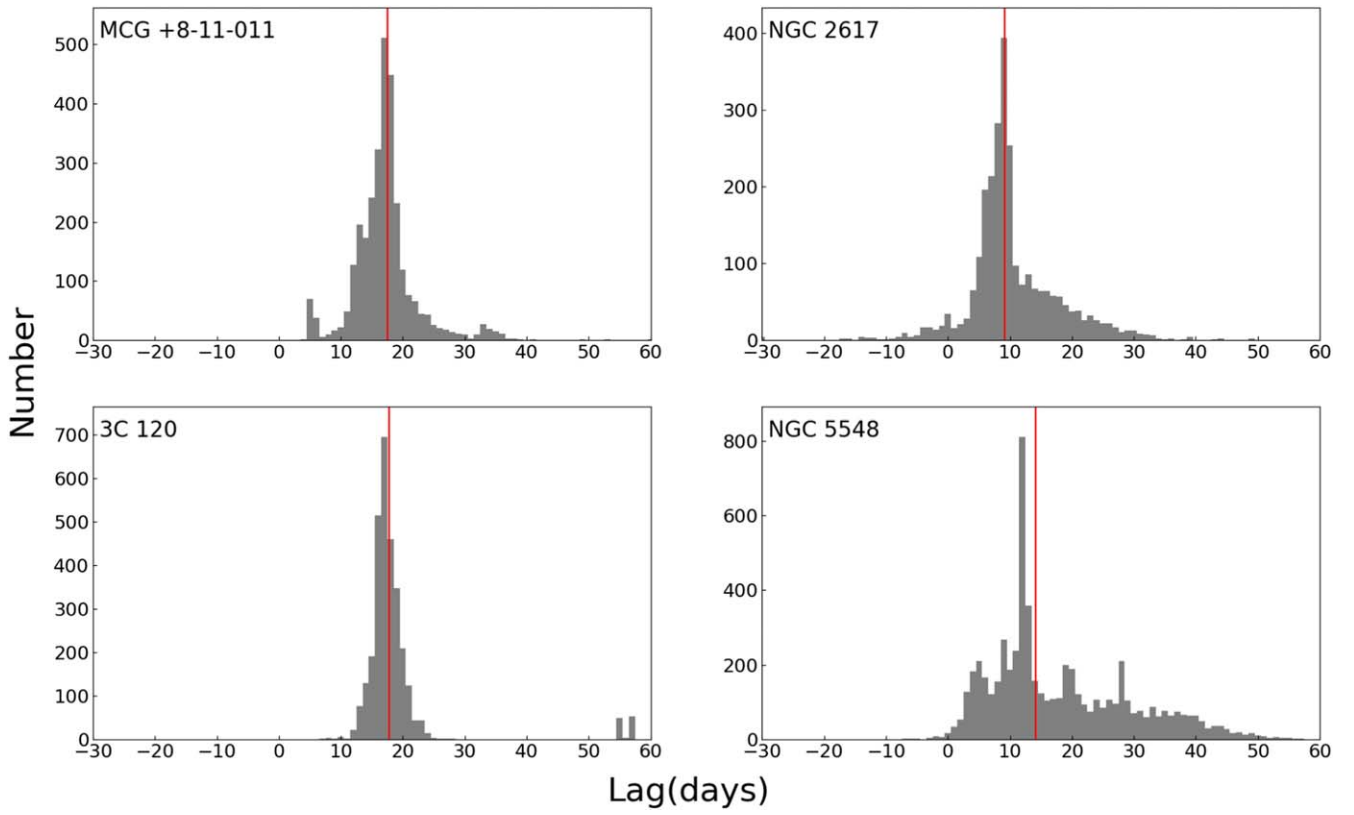
Figure 11. The combined lag distributions for three methods with the same weight. The red lines represent the median lags. For NGC 5548, the panel contains the lag distributions of both the *g*, *r* and *B*, *R* bands.
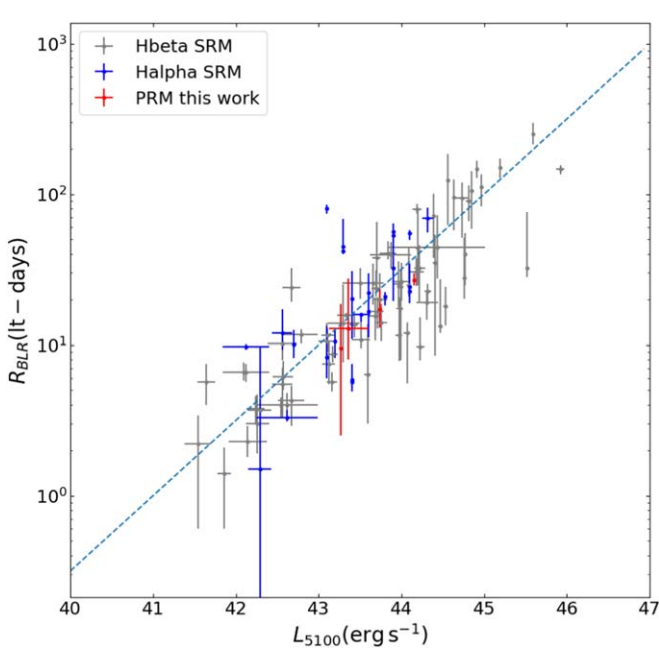

Figure 12. The $R_{BLR} - L_{5100}$ relationship of the broadband PRM, SRM for the Hα line (blue points), and SRM for the Hβ line (black points; Du & Wang 2019). The red points represent the Hα time lags obtained with ICCF-Cut for the *g* and *r* bands. The dashed line is the $R - L$ relation given by Panda et al. (2019).

Figure 13. A comparison of the Hα and Hβ time lags for AGNs with SRM results. The red points are from this work and the blue points are from SRM (Kaspi et al. 2000; Bentz et al. 2010; Grier et al. 2017). The solid line represents the one-to-one ratio.

ICCF-Cut and the χ^2 method for the *g* and *r* bands and the lag distributions of ICCF-Cut and JAVELIN for the *B* and *R* bands are more reliable and consistent with each other.

All Hα lag results (median values) for the four Seyfert 1 galaxies are listed in Table 2. We try to plot the lag distributions of the three methods with the same weight in one figure (Figure 11) and use the highest posterior density to
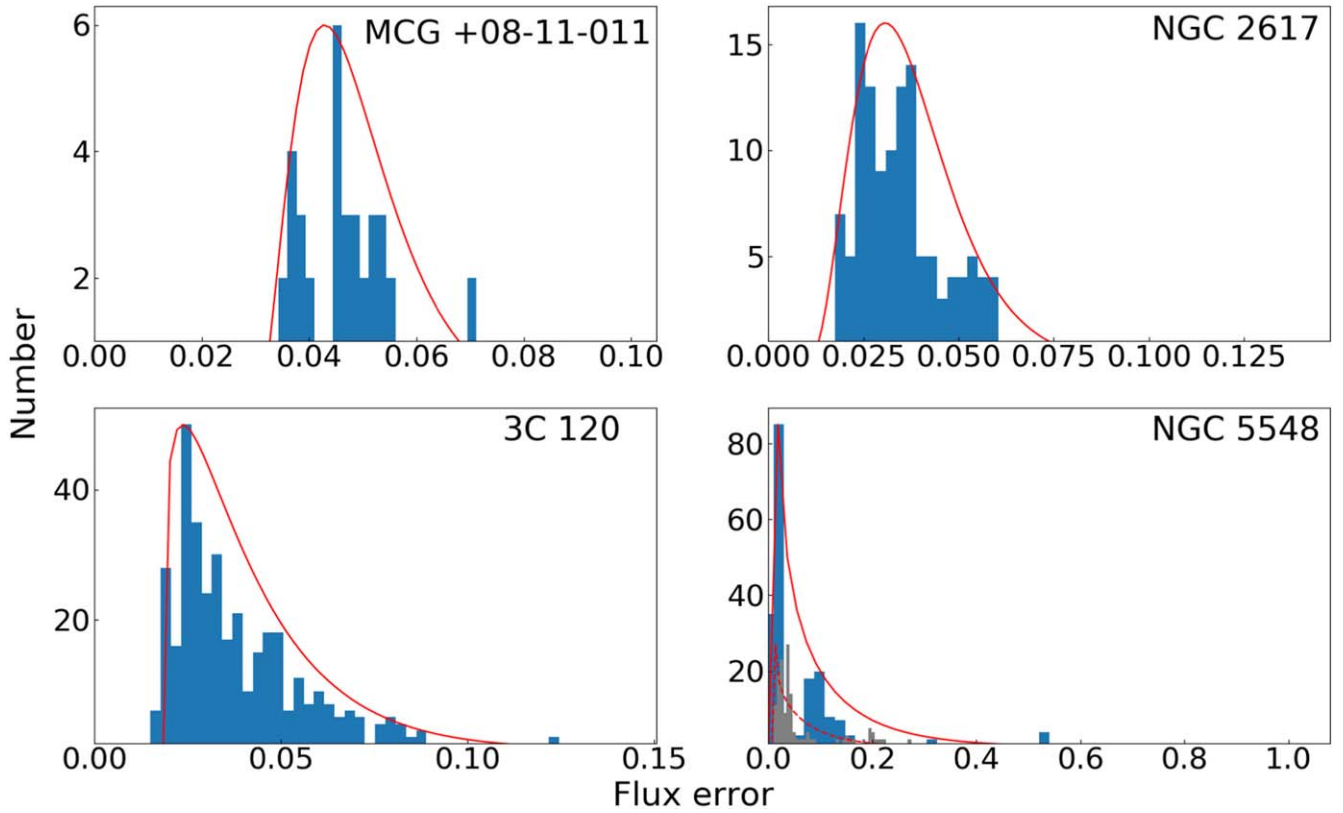
Figure 14. The flux error distributions of the line band for four Seyferts. The blue histograms represent the error distributions of the *r* band and the red lines represent the fittings of their skewed normal distributions. For NGC 5548, the gray histogram and red dashed line represent the data of *R* band.

obtain the lags as a comparison. We find that these combined lags are similar to the ICCF-Cut results. Because the CCF (Blandford & McKee 1982) method has been widely used and examined for decades in many RM projects, we chose the results of ICCF-Cut as the final lags (using the combined lag results gives no significant changes). It is also more convenient to use these lags to compare with other SRM results, which are mainly obtained from the CCF and its variants. We compare our broadband PRM Hα lags with the SRM time lags in the $R - L$ relation (see Figure 12). Our results from the Hα PRM are consistent with the commonly adopted $R_{\rm BLR} \propto L^{\alpha}$ relationship (Panda et al. 2019). We also compare our Hα lag results with those of SRM Hβ lags. Figure 13 shows that on average the Hα time lags are slightly larger than the SRM Hβ time lags, which is consistent with the standard model of AGNs, where the BLR size of the Hα line is usually larger than that of the Hβ line (Kaspi et al. 2000; Bentz et al. 2010; Grier et al. 2012, 2017).

5. Discussion

To examine the reliability of the time lags and the influence of Hβ emission lines in the continuum band, we use the DRW model to produce mock lightcurves of AGNs. The DRW process can be described by a stochastic differential equation (Kelly et al. 2009),

$$dc(t) = -\frac{1}{\tau}c(t)dt + \sigma\sqrt{dt}\,\epsilon(t) + b\tau, \qquad (9)$$

where $c(t)$ is the continuum flux, τ is the relaxation time of the continuum, σ is the standard deviation of the continuum, and $\epsilon(t)$ is a white Gaussian noise process with zero mean and

variance equal to 1. The mean value of the continuum is $b\tau$ and the variance is $\sigma\tau^2/2$. The variability of the broad emission line relative to the continuum can be described as

$$l(t) = \int \Psi(t - t')c(t)dt, \qquad (10)$$

where $\Psi(t)$ is the transfer function between the continuum and the broad emission line. We use a top hat (rectangular function) for the transfer function centered at a time lag τ_d with a width w and an amplitude A:

$$\Psi(t) = \frac{A}{w} \quad \text{for} \quad \tau_d - \frac{w}{2} \leqslant t \leqslant \tau_d + \frac{w}{2}. \qquad (11)$$

Combining the transmission functions of the continuum and line bands and the Hα and Hβ line strengths, as well as the parameters of the AGN lightcurve variability, we can produce mock lightcurves of the continuum and line bands.

We use JAVELIN to obtain the DRW parameters from the observational data of the four Seyfert 1 galaxies, and use these parameters to reproduce the mock lightcurves. We set the Hα and Hβ line strengths obtained from the spectra as the transfer function amplitude. To simulate the observational errors, we use the skewed normal distribution to fit the error distributions for the four sources (see Figure 14) and use the same skewed normal distribution errors to reproduce the mock lightcurves. To simulate the small inter-continuum time lag between the continuum emissions in the continuum and line bands, the mock line band consists of the 1 day lagged continuum and 20 day lagged Hα line.

To make sure the variability of the mock lightcurves is similar to that of the sources, we use the Welch–Stetson *J*
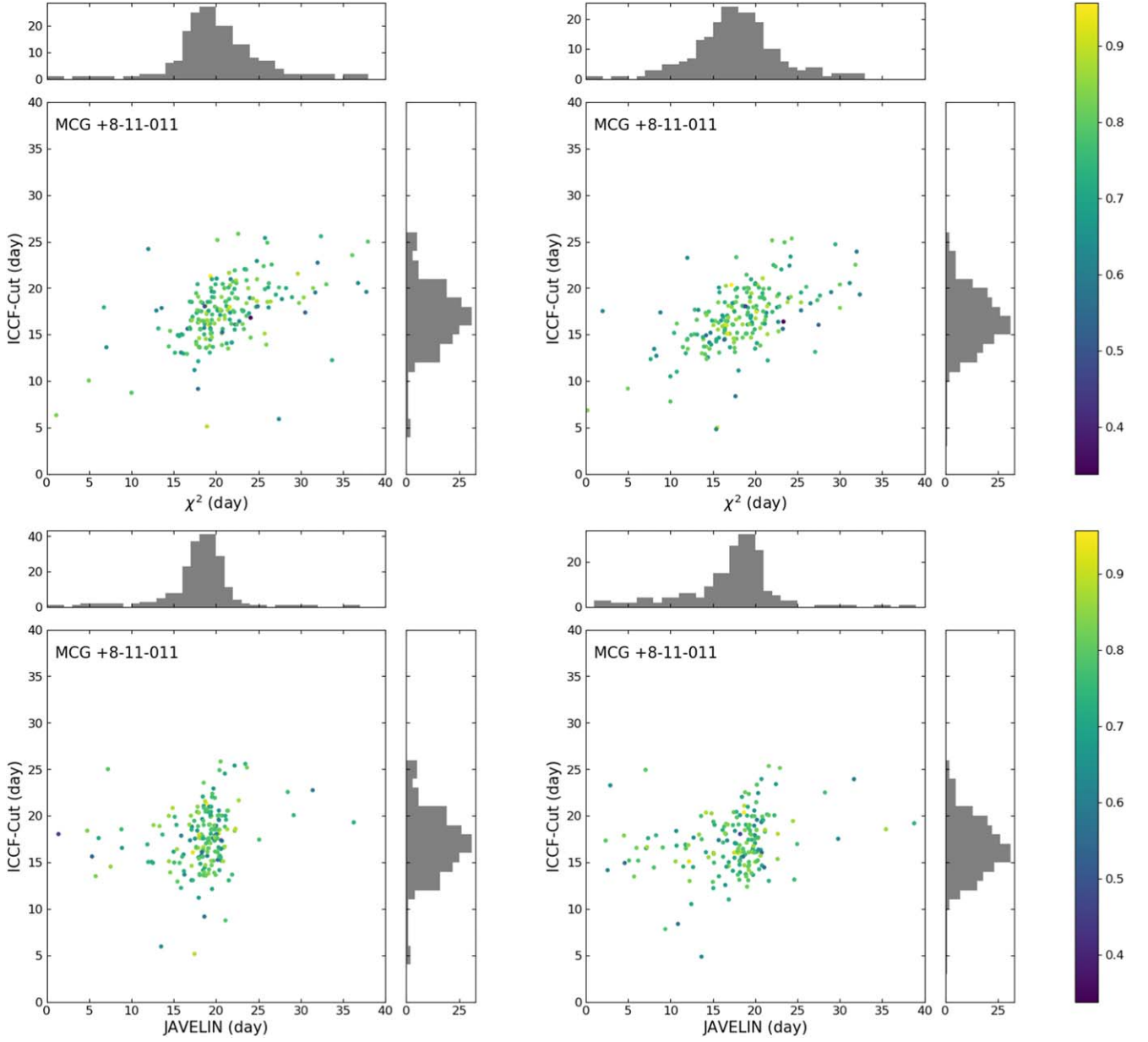
Figure 15. The results of the three methods for 200 mock lightcurves with the initial Hα time lag set as 20 days for MCG+8-11-011. The left panels show the simulations without Hβ line contribution in the continuum band, and the right panels show the simulations with Hβ line contribution in the continuum band and 1 day continuum lag in the line band. The colors of the points represent the peak values of the cross-correlation coefficient r for ICCF-Cut.

Variability Index (Welch & Stetson 1993) to evaluate the variability. The J index is composed of the relative error (δ), the normalized residuals of a pair of observations (P_k), and a weighting factor (w_k). The relative error is defined by Stetson (1996) as

$$\delta_i = \frac{f_i - \overline{f}}{\sigma_{f,i}} \sqrt{\frac{n}{n-1}}. \tag{12}$$

Here, n is the number of observations, $\sigma_{f,i}$ is the measurement error, and $\overline{f}$ is the mean flux of the lightcurve. To reduce the influence of very large flux change within few data points, the weight factor is defined as

$$w_i = \left[1 + \left(\frac{\delta_i}{2}\right)^2\right]^{-1}. \tag{13}$$

The J index is defined as

$$J = \frac{\sum w_k \operatorname{sgn}(\delta_i^2 - 1)\sqrt{|\delta_i^2 - 1|}}{\sum w_k}. \tag{14}$$

Here, "sgn" simply returns the sign of the value. $J < 0$ means that the variability is dominated by the uncertainties of the observation. After reproducing the mock lightcurves with the DRW model, we select the mock lightcurves that have J indexes similar to the real observational data.

For each set of parameters, we use the DRW model to reproduce four mock lightcurves in one simulation. One pair of lightcurves comprises those of the (pure) continuum-band continuum and the line-band continuum with the Hα emission line. This pair of lightcurves represents the ideal data for calculating the time lag with the ICCF-Cut, JAVELIN, and χ^2
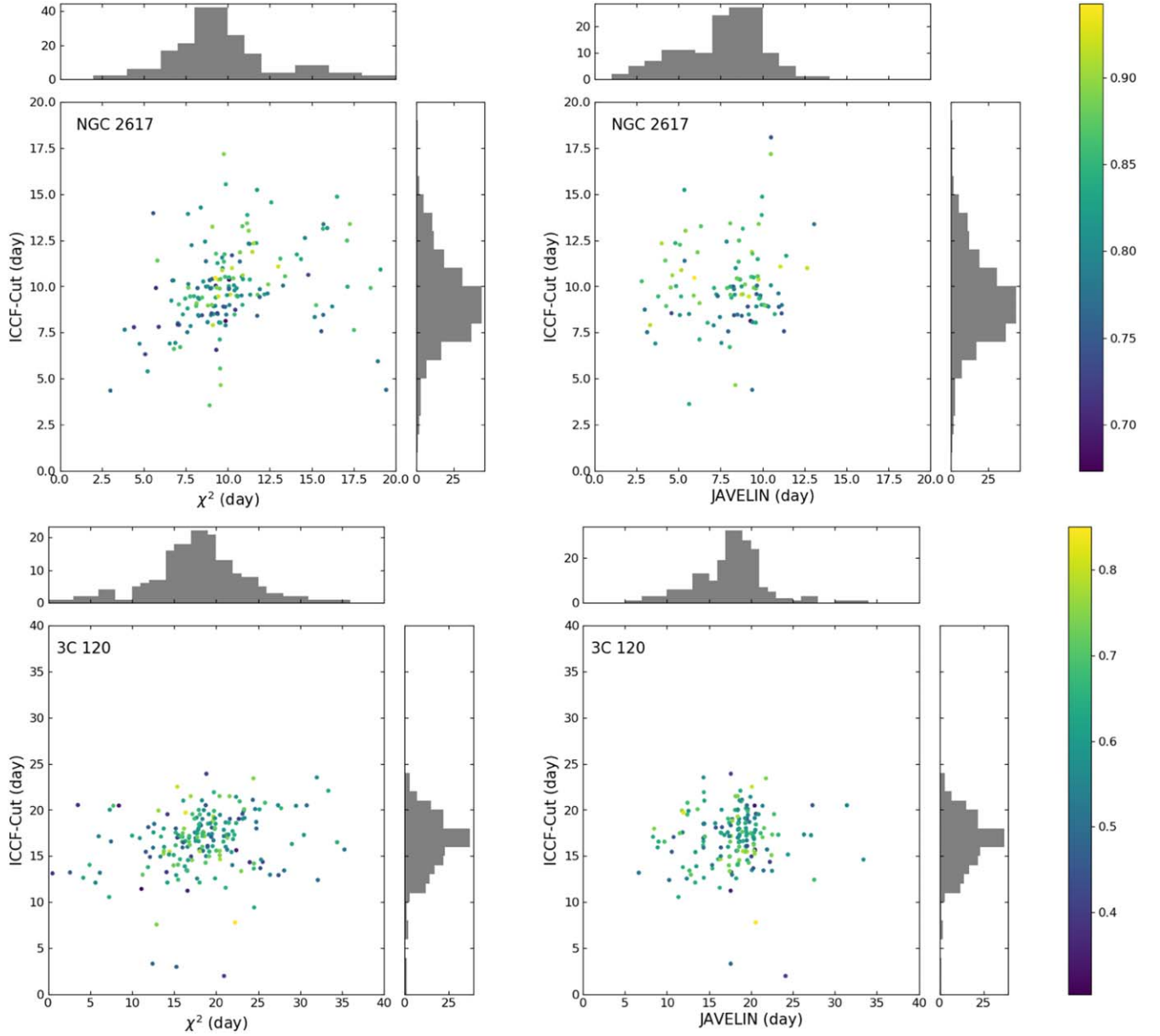
Figure 16. The results of the three methods for NGC 2617 and 3C 120. The left panels show the results of the ICCF-Cut and χ^2 methods, and the right panels show the results of ICCF-Cut and JAVELIN. The colors of the points represent the peak values of the cross-correlation coefficient r for ICCF-Cut.

methods. To simulate the small inter-continuum time lag between the continuum emissions in the continuum and line bands and evaluate the influence of the Hβ line in the continuum band, the mock continuum band consists of the continuum and the 15 day lagged Hβ line, while the mock line band consists of the 1 day lagged continuum and the 20 day lagged Hα line for MCG+8-11-011.

We simulate 200 pairs of mock lightcurves that have similar parameters as MCG+8-11-011, such as the cadence, variabilities, Hα line strength in the line band, and Hβ line strength in the continuum band. Then we use three methods to calculate the time lags for each pair of mock lightcurves and get the distributions of the Hα time lag (see Figure 15). By comparing the left and right panels of Figure 15, we find that although the Hβ line and inter-continuum lag can slightly influence the lag distributions, most of the lags estimated by the three methods are clustered around the true lag of 20 days, indicating that the three methods are efficient for the broadband PRM and the

influence of the Hβ emission line and the inter-continuum lag can be ignored for the Hα lag calculations. From the top panels of Figure 15, it can be noticed that the results of the ICCF-Cut and χ^2 methods have positive correlations, which means that we may obtain similar but not independent lag distributions with the ICCF-Cut and χ^2 methods. By only relying on the consistency of the results with the ICCF-Cut and χ^2 methods, we may obtain biased results. We still need other methods to confirm the results.

We also apply the simulations with the Hβ emission line and the inter-continuum lag to the other three Seyferts. To investigate the influences of the line lag and cadence, the initial Hα lag is set as 10 days for NGC 2617 as a comparison. From Figure 16, we find that for the sources with small lags, like NGC 2617, the dispersion and uncertainty are large. We need a higher cadence to obtain reliable results for AGNs with smaller BLR sizes. From Figure 17, we also find that for NGC 5548, some results of JAVELIN are much smaller than the
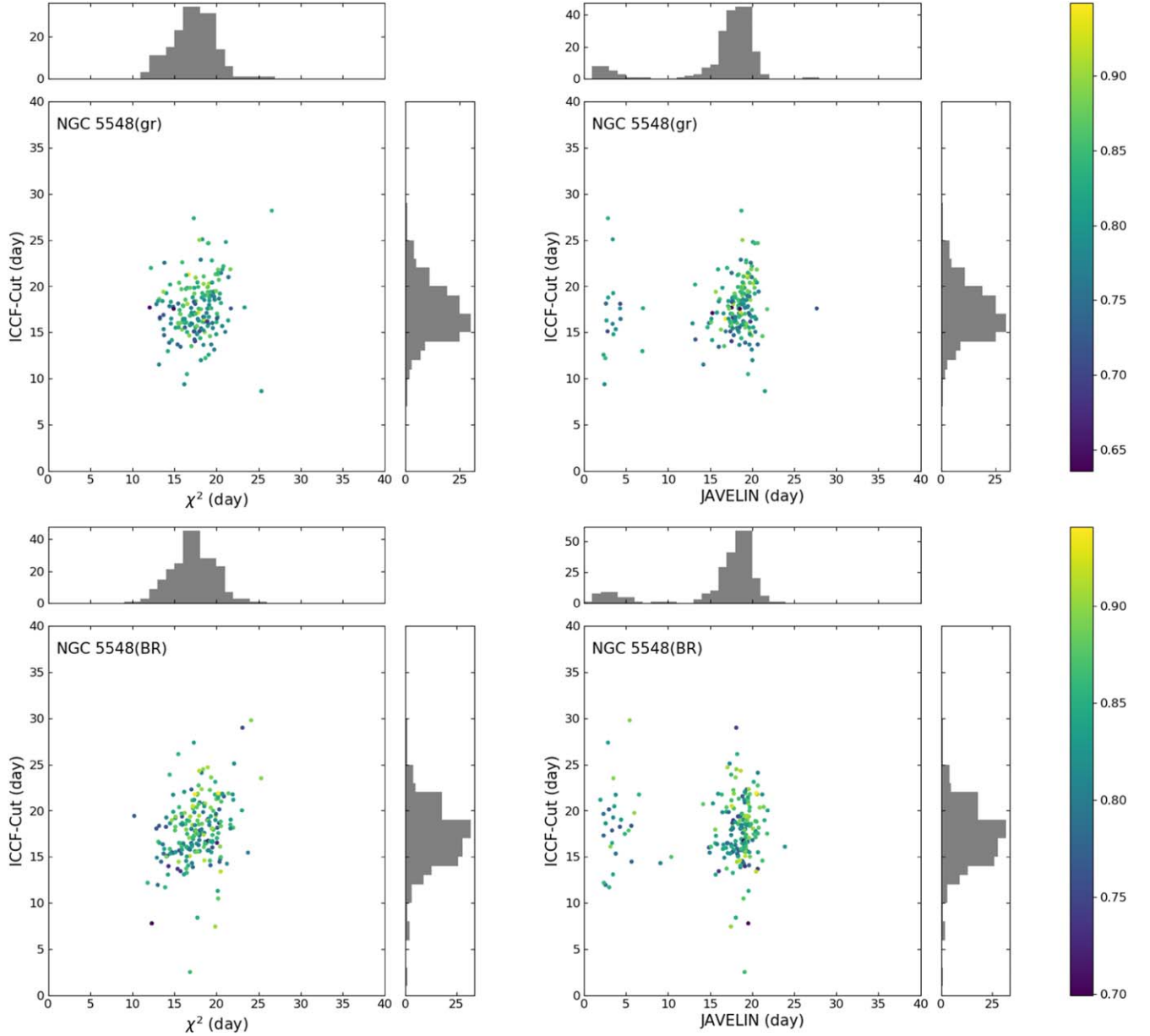
Figure 17. Same as Figure 16, but for NGC 5548. The two top panels represent the results of the *g* and *r* bands. The two bottom panels represent the results of the *B* and *R* bands.

setting lags. The reason may be because the *J* index of NGC 5548 (around 1.0) is smaller than those of the other three Seyferts (2.0~3.0), which means that the variability is smaller than that of the other three Seyferts. This may explain the small Hα lag results of JAVELIN for NGC 5548 (panel (f) of Figure 9). This also means that although the dispersion of the simulative lag distributions for JAVELIN is smaller than those of the ICCF-Cut and χ^2 methods, only relying on the results of JAVELIN may cause problems. Based on the above simulations, we find that using a single method for the broadband PRM may not be very convincing in some cases. We need to use multiple methods to obtain the time lags. The consistency of the lag distributions from different methods can ensure the reliability of the results.

JAVELIN also provides the DPmap model, which can be used to calculate the continuum time lag between the continuum and line bands as well as the Hα line lag. We can compare the Hα time lag and continuum lag obtained from the DPmap with the results in Section 4 and the continuum lag in Fausnaugh et al. (2018). The DPmap model assumes that the *r* band has two components with different time lags. In the MCMC processes, we only request one component to have a $-10 \sim 10$ day time lag, which can be regarded as the inter-continuum lag between the *g* and *r* bands. The results for MCG +8-11-011 are shown in Figure 18 as an example. The DPmap model for MCG+8-11-011 shows a similar Hα time lag distribution at $18.4^{+2.4}_{-6.0}$ days, as shown in Figure 6 and Table 2. The ratios between the line and continuum transfer function amplitude given by the DPmap model are close to the real Hα emission line-to-continuum ratio observed in the line band. The continuum lag distribution of $0.5^{+0.2}_{-0.3}$ days is slightly shorter than the inter-continuum lag between the *g* and *r* bands for the ICCF (about 1.7 days) in Fausnaugh et al. (2018). This may be
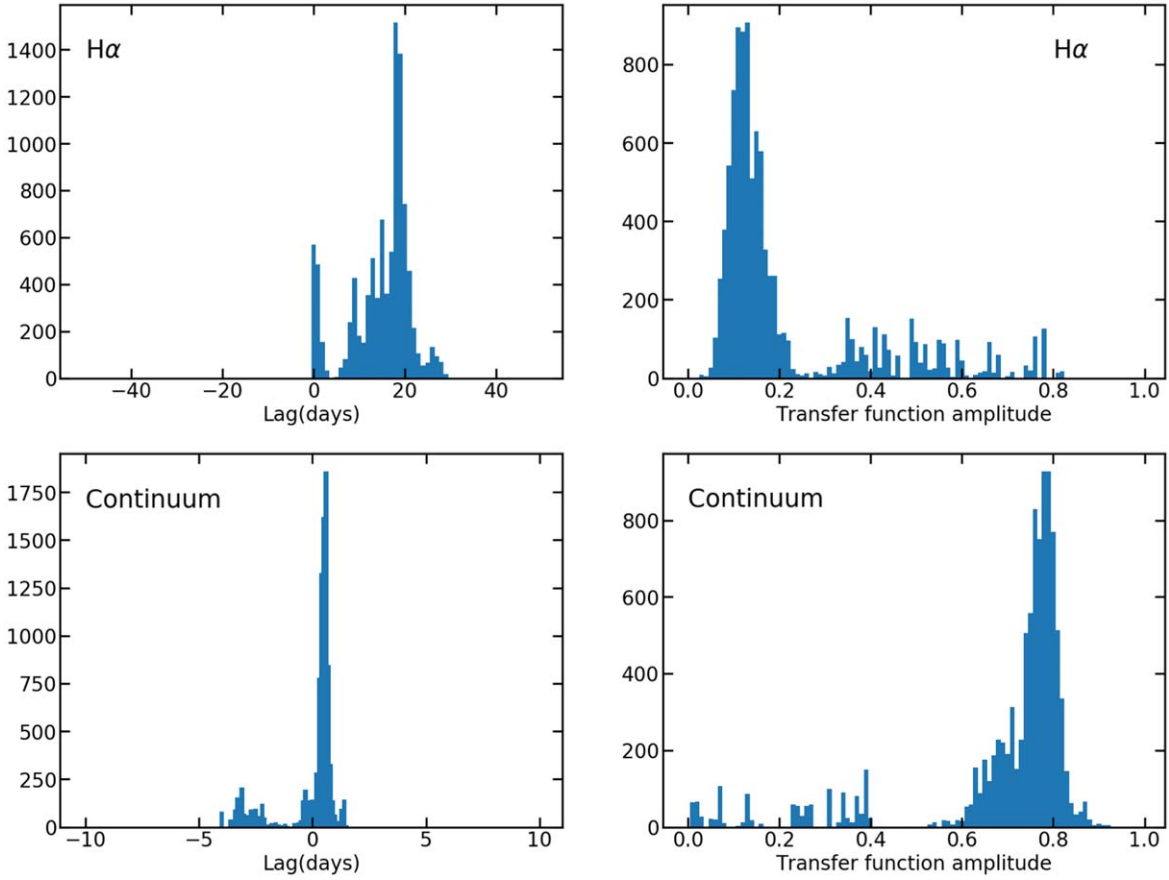
Figure 18. The JAVELIN DPmap model results for MCG+08-11-011. The left panels show the lag distributions and the right panels show the line or continuum strength ratio distributions. The upper left panel represents the Hα lag and the bottom left panel represents the inter-continuum lag between the g and r bands. The initial lag limits are set to $-50 \sim 50$ days for the broad emission line and $-10 \sim 10$ days for the inter-continuum lag. The DPmap model lag is $18.4^{+2.4}_{-6.0}$ days and the inter-continuum lag is $0.5^{+0.2}_{-0.3}$ days.

because the DPmap model includes more parameters than the Pmap model for the same initial data, and the DPmap model is more sensitive to the data quality and tends to yield worse results than the Pmap model. Another reason is that the continuum lags for these local Seyfert 1 AGNs are very small, even smaller than the observational cadence. It is necessary to have a very high cadence and accuracy to obtain the continuum lag and Hα lag simultaneously from the line band. The consistency of the Hα lag results of the DPmap model with the results shown in Figure 6 and Table 2 indicates that the influence of the continuum lag in the line band is insignificant and can be ignored for these Seyfert 1 galaxies.

According to the DRW model, the transfer function amplitude (which can be represented by the statistical mean of the Hα line contribution in the line band) changes very little, but there is a time lag between the Hα and the continuum, so the contribution of the Hα in the line band is not constant. Although we use the minimum function in Equation (4), to make sure the calculated Hα lightcurve contains all the contributions of the Hα emission line, it still needs to evaluate the change of the Hα ratio for the broadband PRM. According to the Hα ratio in the line band obtained from the single-epoch spectrum (as shown in Table 1), we change the Hα ratio from 0.2 to 0.3 with a bin size of 0.01 for MCG+8-11-011, 3C 120, and NGC 5548, and from 0.1 to 0.2 with a bin size of 0.01 for NGC 2617. For each Hα ratio value, we use ICCF-Cut to calculate the lag distribution with FR/RSS, then combine all

the lag distributions to calculate the median value of the lag with highest posterior density. In Figure 19, MCG+8-11-011, NGC 2617, and 3C 120 show lag distributions that are consistent with the results presented in Section 4. For NGC 5548, because of the larger uncertainties in the initial photometric data, the median lag is much larger than the results shown in Table 2, but the peak value $13.0^{+48.0}_{-3.1}$ days of the lag distribution for NGC 5548 is very close to the previous results. These consistencies indicate that using the minimum function in Equation (4) is efficient for the Hα broadband PRM.

6. Summary

By assuming that the continuum flux in the line band equals a fraction of that in the continuum band, we use the modified method of ICCF (ICCF-Cut) to calculate the Hα emission-line time lags from the lightcurves in the continuum and line broad bands. We also consider the host galaxy contribution to the broad bands and the change of the α value for AGNs with longer observational durations to improve the lag results. The lightcurves of extracted Hα are similar to the lagged continuum-band lightcurves and the lagged simultaneous SRM Hβ lightcurves.

To evaluate the influence of the errors of the extracted Hα lightcurves and the feasibility of the Hα broadband PRM with large uncertainties, we apply the χ^2 method to weigh the points
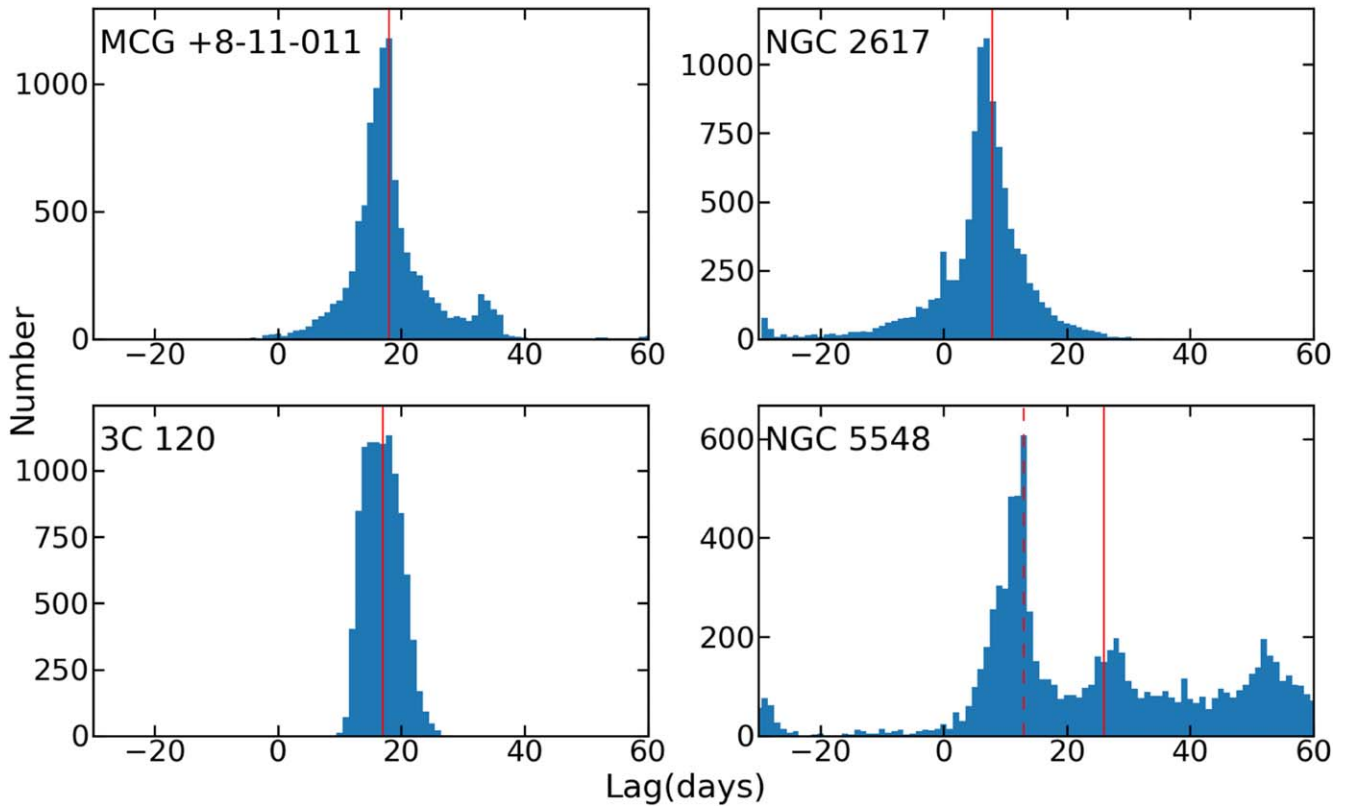
Figure 19. The ICCF-Cut lag distributions with different values of α for four Seyfert 1 galaxies. The red line represents the median value of the lag distribution. The Hα lags are $18.0^{+6.5}_{-4.5}$ days for MCG+8-11-011, $7.8^{+4.2}_{-5.7}$ days for NGC 2617, $17.0^{+3.8}_{-3.1}$ days for 3C 120, and $26.0^{+35.2}_{-16.1}$ days for NGC 5548, respectively. For NGC 5548, the red dashed line represents the peak value of the lag distribution, which is $13.0^{+48.0}_{-3.1}$ days.

in lightcurves by the uncertainties. By combining the results of the ICCF-Cut, JAVELIN, and χ^2 methods, we find that the derived Hα time lags for four Seyfert 1 galaxies are consistent with the $R - L$ relationship obtained from the SRM. These AGNs show slightly larger Hα lags from the broadband PRM than Hβ lags from the SRM, which is consistent with previous works and theoretical predictions that the BLR size of the Hα line is usually larger than that of the Hβ emission line.

To confirm our results further, we use the DRW model to simulate mock lightcurves that have similar parameters to our selected AGNs. By calculating the time lags of these mock lightcurves, we evaluate the reliability of the time lags obtained from the Hα broadband PRM and the influences of the Hβ line in the continuum band. By comparing the results of the JAVELIN DPmap model with previous results, we find that the continuum lag in the line band can be ignored in broadband PRM for these local Seyfert 1 galaxies whose continuum lags are very small. By calculating the Hα lags with different Hα ratios, we find that using the minimum function in Equation (4) is efficient for the Hα broadband PRM.

From the comparisons of the results from the Hα broadband PRM and SRM and the results of the simulations, we find that the consistency of the ICCF-Cut, JAVELIN, and χ^2 methods can ensure the reliability of the Hα line lags obtained from the broadband PRM. However, we must admit that all four Seyfert 1 galaxies have high-quality broadband lightcurves with daily/subdaily cadences, which enables us to get reliable Hα lags. It is difficult to do so for other AGNs with poor-quality broadband data. We expect that these broadband PRM methods will be able to be used to study the BLR sizes and BH masses of a large sample of AGNs in the era of large multi-epoch and

high-cadence photometric sky surveys such as ZTF (Masci et al. 2019) and LSST (LSST Science Collaboration et al. 2017) in the near future.

ORCID iDs

Qinchun Ma ◉ https://orcid.org/0000-0003-0827-2273
Xue-Bing Wu ◉ https://orcid.org/0000-0002-7350-6913
Yuming Fu ◉ https://orcid.org/0000-0002-0759-0504

References

Bao, D.-W., Brotherton, M. S., Du, P., et al. 2022, ApJS, 262, 14
Bentz, M. C., Denney, K. D., Cackett, E. M., et al. 2007, ApJ, 662, 205
Bentz, M. C., Peterson, B. M., Pogge, R. W., & Vestergaard, M. 2009, ApJL, 694, L166
Bentz, M. C., Peterson, B. M., Pogge, R. W., Vestergaard, M., & Onken, C. A. 2006, ApJ, 644, 133
Bentz, M. C., Walsh, J. L., Barth, A. J., et al. 2010, ApJ, 716, 993
Blandford, R. D., & McKee, C. F. 1982, ApJ, 255, 419
Brown, T. M., Baliber, N., Bianco, F. B., et al. 2013, PASP, 125, 1031
Choloniewski, J. 1981, AcA, 31, 293
Cid Fernandes, R., Sodré, L. J., & Vieira da Silva, L. J. 2000, ApJ, 544, 123
Collin, S., Kawaguchi, T., Peterson, B. M., & Vestergaard, M. 2006, A&A, 456, 75
Czerny, B., Hryniewicz, K., Maity, I., et al. 2013, A&A, 556, A97
Denney, K. D., Peterson, B. M., Pogge, R. W., et al. 2009, ApJL, 704, L80
Du, P., & Wang, J.-M. 2019, ApJ, 886, 42
Edri, H., Rafter, S. E., Chelouche, D., Kaspi, S., & Behar, E. 2012, ApJ, 756, 73
Fausnaugh, M. M., Denney, K. D., Barth, A. J., et al. 2016, ApJ, 821, 56
Fausnaugh, M. M., Grier, C. J., Bentz, M. C., et al. 2017, ApJ, 840, 97
Fausnaugh, M. M., Starkey, D. A., Horne, K., et al. 2018, ApJ, 854, 107
Feng, H.-C., Liu, H. T., Bai, J. M., et al. 2021, ApJ, 912, 92
Gaskell, C. M., & Sparke, L. S. 1986, ApJ, 305, 175
Graham, A. W., Onken, C. A., Athanassoula, E., & Combes, F. 2011, MNRAS, 412, 2211
Grier, C. J., Pancoast, A., Barth, A. J., et al. 2017, ApJ, 849, 146
Grier, C. J., Peterson, B. M., Horne, K., et al. 2013, ApJ, 764, 47
Grier, C. J., Peterson, B. M., Pogge, R. W., et al. 2012, ApJ, 755, 60
Haas, M., Chini, R., Ramolla, M., et al. 2011, A&A, 535, A73
Hlabathe, M. S., Starkey, D. A., Horne, K., et al. 2020, MNRAS, 497, 2910
Homayouni, Y., Trump, J. R., Grier, C. J., et al. 2019, ApJ, 880, 126
Horne, K., De Rosa, G., Peterson, B. M., et al. 2021, ApJ, 907, 76
Jiang, L., Shen, Y., McGreer, I. D., et al. 2016, ApJ, 818, 137
Kammoun, E. S., Papadakis, I. E., & Dovčiak, M. 2021, MNRAS, 503, 4163
Kaspi, S., Smith, P. S., Maoz, D., Netzer, H., & Jannuzi, B. T. 1996, ApJL, 471, L75
Kaspi, S., Smith, P. S., Netzer, H., et al. 2000, ApJ, 533, 631
Kawaguchi, T., Mineshige, S., Umemura, M., & Turner, E. L. 1998, ApJ, 504, 671
Kelly, B. C., Bechtold, J., & Siemiginowska, A. 2009, ApJ, 698, 895
Kim, J., Im, M., Choi, C., & Hwang, S. 2019, ApJ, 884, 103
Kollatschny, W., Ulbrich, K., Zetzl, M., Kaspi, S., & Haas, M. 2014, A&A, 566, A106
Koratkar, A. P., & Gaskell, C. M. 1991, ApJL, 370, L61
Labita, M., Treves, A., Falomo, R., & Uslenghi, M. 2006, MNRAS, 373, 551
Landt, H., Ward, M. J., Kynoch, D., et al. 2019, MNRAS, 489, 1572
LSST Science Collaboration, Marshall, P., Anguita, T., et al. 2017, arXiv:1708.04058
Lu, K.-X., Du, P., Hu, C., et al. 2016, ApJ, 827, 118
Masci, F. J., Laher, R. R., Rusholme, B., et al. 2019, PASP, 131, 018003
McGill, K. L., Woo, J.-H., Treu, T., & Malkan, M. A. 2008, ApJ, 673, 703
Netzer, H. 1990, in Saas-Fee Advanced Course of the Swiss Society for Astrophysics and Astronomy: Active Galactic Nuclei, ed. R. D. Blandford et al., 57
Onken, C. A., Ferrarese, L., Merritt, D., et al. 2004, ApJ, 615, 645
Panda, S., Martínez-Aldama, M. L., & Zajaček, M. 2019, FrASS, 6, 75
Pei, L., Fausnaugh, M. M., Barth, A. J., et al. 2017, ApJ, 837, 131
Peterson, B. M. 1993, PASP, 105, 247
Peterson, B. M., Berlind, P., Bertram, R., et al. 2002, ApJ, 581, 197
Peterson, B. M., & Wandel, A. 1999, ApJL, 521, L95
Peterson, B. M., Wanders, I., Bertram, R., et al. 1998, ApJ, 501, 82
Planck Collaboration, Ade, P. A. R., Aghanim, N., et al. 2014, A&A, 571, A16
Polletta, M., Tajer, M., Maraschi, L., et al. 2007, ApJ, 663, 81
Pozo Nuñez, F., Ramolla, M., Westhues, C., et al. 2012, A&A, 545, A84
Pozo Nuñez, F., Westhues, C., Ramolla, M., et al. 2013, A&A, 552, A1
Ramolla, M., Haas, M., Westhues, C., et al. 2018, A&A, 620, A137
Sakata, Y., Minezaki, T., Yoshii, Y., et al. 2010, ApJ, 711, 461
Shapovalova, A. I., Popović, L. Č, Collin, S., et al. 2008, A&A, 486, 99
Shappee, B. J., Prieto, J. L., Grupe, D., et al. 2014, ApJ, 788, 48
Shen, Y., Brandt, W. N., Dawson, K. S., et al. 2015, ApJS, 216, 4
Stalin, C. S., Jeyakumar, S., Coziol, R., Pawase, R. S., & Thakur, S. S. 2011, MNRAS, 416, 225
Stetson, P. B. 1996, PASP, 108, 851
Tody, D. 1986, Proc. SPIE, Vol. 627, 733
Tody, D. 1993, in ASP Conf. Ser. 52, Astronomical Data Analysis Software and Systems II, ed. R. J. Hanisch, R. J. V. Brissenden, & J. Barnes (San Francisco, CA: ASP), 173
Urry, C. M., & Padovani, P. 1995, PASP, 107, 803
Vestergaard, M., Denney, K., Fan, X., et al. 2011, in Narrow-Line Seyfert 1 Galaxies and their Place in the Universe, ed. L. Foschini et al., 38
Wandel, A., Peterson, B. M., & Malkan, M. A. 1999, ApJ, 526, 579
Welch, D. L., & Stetson, P. B. 1993, AJ, 105, 1813
Winkler, H., Glass, I. S., van Wyk, F., et al. 1992, MNRAS, 257, 659
Woo, J.-H., Treu, T., Barth, A. J., et al. 2010, ApJ, 716, 269
Woo, J.-H., Yoon, Y., Park, S., Park, D., & Kim, S. C. 2015, ApJ, 801, 38
York, D. G., Adelman, J., Anderson, J. E. J., et al. 2000, AJ, 120, 1579
Yu, Z., Martini, P., Davis, T. M., et al. 2020, ApJS, 246, 16
Zu, Y., Kochanek, C. S., Kozłowski, S., & Peterson, B. M. 2016, ApJ, 819, 122
Zu, Y., Kochanek, C. S., Kozłowski, S., & Udalski, A. 2013, ApJ, 765, 106
Zu, Y., Kochanek, C. S., & Peterson, B. M. 2011, ApJ, 735, 80